Diploma thesis

Growth morphologies of the polar organic molecule dihydrotetraazaheptacene on graphene

by

Guanpeng LIN

at Institute of Physics

Montanuniversität Leoben, Austria

under supervision of

Dr. Aleksandar Matković

Ao. Univ. Prof. Dr. Christian Teichert

refereed by

Ao. Univ. Prof. Dr. Christian Teichert

Leoben, September 2017

EIDESSTATTLICHE ERKLÄRUNG

Ich erkläre an Eides statt, dass ich diese Arbeit selbständig verfasst, andere als die angegebenen Quellen und Hilfsmittel nicht benutzt und mich auch sonst keiner unerlaubten Hilfsmittel bedient habe.

AFFIDAVIT

I declare in lieu of oath, that I wrote this thesis and performed the associated research myself, using only literature cited in this volume.

Datum	Unterschrift

Table of content: (3)

Abstract

The device performance of organic field-effect transistors depends not only on the properties of different functional components, but it is also determined by the interfaces among them. Interface engineering has been demonstrated to be an effective approach to enhance the quality and functionality of organic semiconductor thin films, as an example optimizing the contact with electrodes in order to enable high performance of the final devices. For the past few years, two-dimensional (2D) or van der Waals materials have been suggested as substrates, on which the epitaxy of organic molecules can lead to advanced heterostructures through self-assembly. This is because their surfaces are atomically smooth without dangling bonds and exhibit no trapped charges at the interface. These key advantages enable the growth of high-quality organic crystal thin films with low amount of defects and allow exploitation of the intrinsic properties of organic semiconductors.

This thesis focuses on the epitaxial growth of dihydrotetraazaheptacene (DHTA7), which is a polar and rod-like, small organic semiconductor molecule, on the 2D material graphene. The hot wall epitaxy technique was chosen for the deposition of DHTA7 molecules on micromechanically exfoliated graphene surfaces. As the main characterization tool, atomic force microscopy was used to analyze the morphology of the DHTA7 crystallites on the nanometer scale as a function of deposition temperature from 313 K to 393 K. Optical microscopy was also employed to investigate the micrometer-sized structures.

It was found that the molecules adsorb in flat-lying configuration on graphene forming elongated needle-like crystallites. These crystallites follow certain growth directions that are dictated by the substrate's three-fold symmetry. In total, six growth directions of DHTA7 on graphene were observed, with three pairs of directions split by ± 9° from three armchair directions of graphene. These growth directions can also be used to determine the crystallographic orientation of the substrate and its edges. In addition, the influence of the thickness of supporting graphene was investigated, showing that single-layer graphene is actually not favored for the growth of large and well-ordered crystalline DHTA7 needles.

Kurzfassung

Die Bauelementecharakteristik von organischen Feldeffekttransistoren hängt nicht nur von den Eigenschaften unterschiedlicher Funktionskomponenten ab, sondern wird auch durch die Grenzflächen untereinander bestimmt. Grenzflächenengineering hat sich als eine effektive Möglichkeit zur Erhöhung der Qualität und Funktionalität von organsichen Halbleiterdünnschichten erwiesen, wie das Beispiel der Optimierung des Elektrodenkontakts von high-performance-Bauelementen zeigt. In den vergangenen Jahren wurden zwei-dimensionale (2D) oder van-der-Waals-Materialien als Substrate vorgeschlagen, auf denen die Epitaxie organischer Moleküle durch Selbstorganisation zu verbesserten Heterostrukturen führen kann. Das resultiert aus dem Fakt, dass deren Oberflächen atomar glatt sind ohne freie Bindungen und keine eingeschlossenen Ladungen an der Grenzfläche zeigen. Dies sind entscheidende Vorteile, die das Wachstum von hochwertigen dünnen, organischen Kristallschichten mit geringen Defekten und die Ausnutzung der intrinsischen Eigenschaften von organischen Halbleitern ermöglichen.

Diese Arbeit konzentriert sich auf das epitaktische Wachstum von Dihydrotetraazaheptacen (DHTA7), einem kleinen, polaren und stabförmigen organisches Halbleitermolekül - auf dem 2D Material Graphen. Für die Abscheidung von DHTA7-Molekülen auf mikromechanisch exfolierten Graphenoberflächen wurde die Hot-Wall-Epitaxie-Technik gewählt. Als hauptsächliche Charakterisierungsmethode auf der Nanometerskala wurde die Rasterkraftmikroskopie zur Analyse der Morphologie von DHTA7-Kristalliten als Funktion der Abscheidetemperatur von 313 K auf 393 K verwendet. Weiters wurde optische Mikroskopie zur Untersuchung Mikrometer großen Strukturen eingesetzt.

Es wurde festgestellt, dass die Moleküle in flach liegender Konfiguration auf Graphen adsorbieren und dabei längliche nadelartige Kristallite bilden. Diese Kristallite folgen bestimmten Wachstumsrichtungen, die durch die dreizählige Symmetrie des Substrats vorgegeben sind. Insgesamt wurden sechs Wachstumsrichtungen von DHTA7 auf Graphen beobachtet, wobei drei Richtungspaare auftreten, die um jeweils ± 9 ° von den drei „Armchair“ Richtungen von Graphen abweichen. Diese Wachstumsrichtungen können auch verwendet werden, um die kristallographische Orientierung des Substrats und seiner Kanten zu bestimmen. Darüber hinaus wurde der Einfluss der Dicke des Graphensubstrats untersucht, wobei sich zeigte, dass einlagiges Graphen nicht vorteilhaft ist für das Wachstum von großen und gut geordneten kristallinen DHTA7-Nadeln.

1. Introduction

Graphene – a single atomic layer of graphite – was for the first time isolated in 2004 [1], and only 6 years later Andre Geim and Konstantin Novoselov have received a Nobel Prize in physics for the ground-breaking research on this two-dimensional (2D) material. This discovery started a whole new field of physics related to 2D materials [2]. It is expected that graphene will contribute significantly to flexible and wearable electronic devices in the next decade [3]. Because of its promising electronic and mechanical properties with high optical transmittance, graphene can be treated as a high-quality material to fabricate flexible transparent conducting electrodes [3].

Graphene has no band-gap and for almost all potential electronic applications materials with band gaps – usually in the visible range – are needed. For this reason, graphene was integrated with many different semiconducting technologies as silicon, III-V semiconductors, 2D semiconductors (e.g. transition metal dichalcogenides like MoS_2), organic semiconductors, and many other [3]. In the case of organic thin-films, in particular for solar cell applications, use of inexpensive organic polymers instead of the expensive crystalline silicon leads to a lower fabrication cost. Furthermore, the polymers can be processed by low-cost equipment to make photographic films (i.e. thin-film-technologies), which represents an advantage on cost in comparison with conventional manufacturing through expensive growth methods as molecular beam epitaxy or chemical vapor deposition [4]. These organic solar cells (OSC) utilize organic photovoltaic materials and organic semiconductor diode-like structures in order to convert light into electricity. An organic light-emitting diode (OLED) consists of a thin film of organic material that emits light under stimulation by an electric current. An organic field-effect transistor (OFET) is a FET utilizing similar to OSCs and OLEDs organic molecules or polymers as the active semiconducting layer.

Unlike silicon-based technologies, organic thin-films are highly sensitive to the type and quality of the surfaces on which they are grown. Although promising to reach high-performance, these organic films are usually hindered by technical issues related to contact quality or the quality of film grown on a thin gate dielectric of an OFET. It is known that a high amount of defects and grain boundaries in the grown organic films severely affects the resulting device performance. That is where van der Waals (vdW)– or 2D – materials could be used to overcome technological issues. Growing molecules on van der Waals substrates enables a significant enhancement in the final device performance, e.g. by optimizing the gate organic semiconductor interface only in the first few molecular layers where most of the current flows [5] and also exhibit a major impact on stability of the contact and active area [6], since the number of defects and grain boundaries are reduced, and these usually play a major role in the degradation of organic thin-films.

2. Theoretical background

2.1. Graphene

Graphene, as its name indicates, is extracted from graphite which is the material used in pencils. Graphene is an allotrope of carbon, meaning that it is entirely composed of carbon atoms like graphite. Graphite is a three-dimensional crystalline arrangement, while graphene is a 2D crystal with only one atom thickness. 1 mm thick graphite contains about 3 million layers of graphene. The carbon atoms among them are perfectly distributed in a hexagonal formation about only 0.3 nm thick which is presented in figure 1.

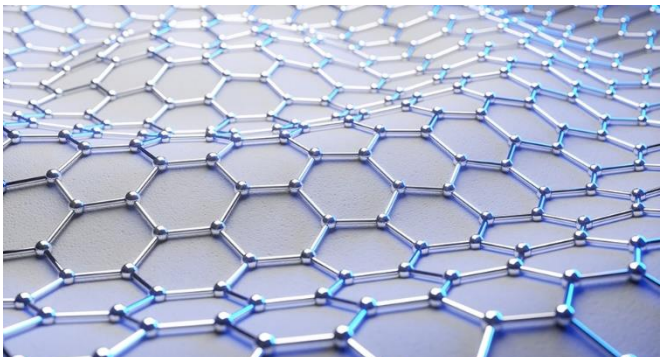

Figure 1: Crystalline structures of graphene [7]

Graphene exhibits a series of unusual properties. It efficiently conducts electricity better than copper, and is 200 times stronger than the strongest steel but six times lighter [8]. Since it absorbs only 2% of light [9], it is nearly fully transparent. Furthermore, chemical components can be added to its surface to change its properties.

In fact, wide-spread appreciation of this special material has come a long way. At the beginning, graphene was believed to be unstable. Since it was later isolated and characterized through electronic measurements by two scientists in 2004 [1], graphene became more and more favorable. Although, it should be mentioned that surface scientists have prepared atomically thin graphite on single crystalline metal support already decades earlier. Being a good conductor and at the same time almost completely transparent, graphene is a potential candidate to replace indium-tin-oxide in flat-screen technologies, OLEDs, OSCs, and touchscreens [3]. Furthermore, since graphene is made from carbon, it is very light while still being one of the hardest materials known. For this reason, graphene is expected to be integrated into many composite materials and alloys, e.g., to eliminate the impact of lightning on aircraft fuselages [10]. Recently, "dye-sensitized solar cells were fabricated using graphene-TiO_2 composite photoanodes. The graphene-TiO_2 nanocomposites were prepared using the heterogeneous coagulation between Nafion-coated graphene and commercial TiO_2 nanoparticles, which ensured a tight interfacial binding between them" [11].

2.2 Interfaces between graphene and organic semiconductors

As a potential transparent electrode material in organic electronics, graphene exhibits crucial advantages in addition to those properties such as high mechanical strength, high transparency, flexibility, thermal and chemical stability that have been mentioned in the previous chapters. Specific advantages to use graphene as an electrode are based on the favorable band alignment with many organic semiconductors. Also, organic semiconductor growth morphologies on top of graphene have larger grains and lower amount of defects compared to usually used sputtered metal electrodes. This is due to the van der Waals interface between graphene and organic semiconductors [12]. As a result, these heterostructures consisting of organic semiconductors and graphene are applied for low injection barriers, high charge extractions, and high injection efficiencies. They also exhibit an ability to preserve the intrinsic functionality of the organic semiconductors at the interface.

Graphene was for the first time reported in 2008 as a carrier injection layer between small-molecule films and metallic contacts [13] where favorable band alignment has allowed for a large reduction of the contact resistance between electrodes and the active organic layer of a OFET. Afterwards, only graphene was used as an electrode without the underlying metal since only one layer of graphene has sufficiently high conductivity to replace common metal electrodes as copper or even gold [14-16].

Since graphene was proven as a suitable electrode material for organic semiconductors [13-16], proof-of-concept organic light-emitting diodes were also made using graphene instead of indium-tin-oxide as a transparent anode [17-21]. Even photo-transistors – using light pulses as gate signal – have been realized with the interfaces between graphene and organic semiconductors [22]. All of these novel applications of the interfaces between graphene and organic semiconductors highlight their importance for the emerging technologies as flexible and wearable electronics, flexible displays, organic solar cells, and many other.

3. Materials and methods

3.1 DHTA7 and hydrogen bonding

Dihydrotetraazaheptacene (DHTA7) consists of seven phenyl rings connected by their common edges forming a rod-like structure with two H-donor (N-H) and two H-acceptor (N=C) groups. The whole backbone obtains a length of about 2 nm. Figure 2 shows the molecular structure of an individual molecule of this polymer. This acene derived molecule has been realized within the Framework of an Austrian french research project FWF I1788-N20 in the group of Olivier Siri, CINAM-CNRS, Aix - Marseille - University.

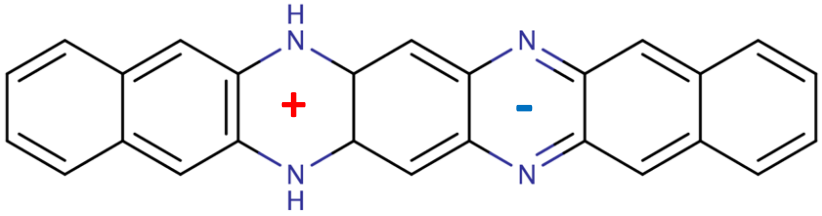

Figure 2: Structure of a DHTA7 molecule indicating the dipole

For charge to be able to propagate in a band-like manner between the molecules it is needed that molecular π-orbitals overlap to an extent [23]. Therefore, in amorphous or polycrystalline films, the charge carrier mobility is severely reduced due to defect induced lack of orbital overlap. Thus, enhancing carrier mobility in thin-film organic semiconductor devices – and approaching intrinsic properties of the organic semiconductors – is mainly dependent on long-range ordering [24]. As an example, pentacene is one of the most studied organic semiconductors since high orbital-overlap in pentacene single-crystals enables high intrinsic mobility. However, pentacene has long-term structural stability issues, since it suffers from low thermal stability, and photooxidation [25]. These stability drawbacks of pentacene have motivated the research for nitrogen-containing derivates of azenes in an effort to resolve the instability issues under ambient conditions, while keeping a similar backbone of the molecule [26]. More specifically, dihydrotetraazapentacene (DHTAP) derivative has two different types of nitrogen based groups substituting four of its carbon atoms. These groups enhance stability of the molecular crystals through dipolar interactions and hydrogen bridges which govern the molecular arrangement in the bulk [27].

Having a similar structure of DHTAP, dihydrotetraazaheptacene (DHTA7) exhibits two additional phenyl rings on both side of its backbone. The growth of well-ordered azaheptacene films seems to be an important challenge. Similar to DHTAP, two H-donor (N-H) and two H-acceptor (N=C) sites are expected to stabilize the bulk structure through hydrogen bridges and dipolar interaction [28], DHTA7 may like DHTAP appear to afford a good choice for the growth of well-ordered molecular layers.

Understanding the nucleation and orientation of the organic molecules on top of a substrate is very important to improve the performance of devices. The interaction with the substrate usually governs the molecular orientation of the first few layers, which would then influence the growth morphology of the entire film. If the samples-substrate interaction reaches a minimal value, island-like structures consisting of nearly upright standing molecules are formed. On the other side, if the maximal sample-substrate interaction is reached, it forms needle-like structures consisting of flat-lying molecules. Figure 3 represents the cases providing growth morphologies together with molecular structure as obtained by Prof. P. Puschnig, Karl – Franzens – University Graz employing density functional theory (DFT) calculations.

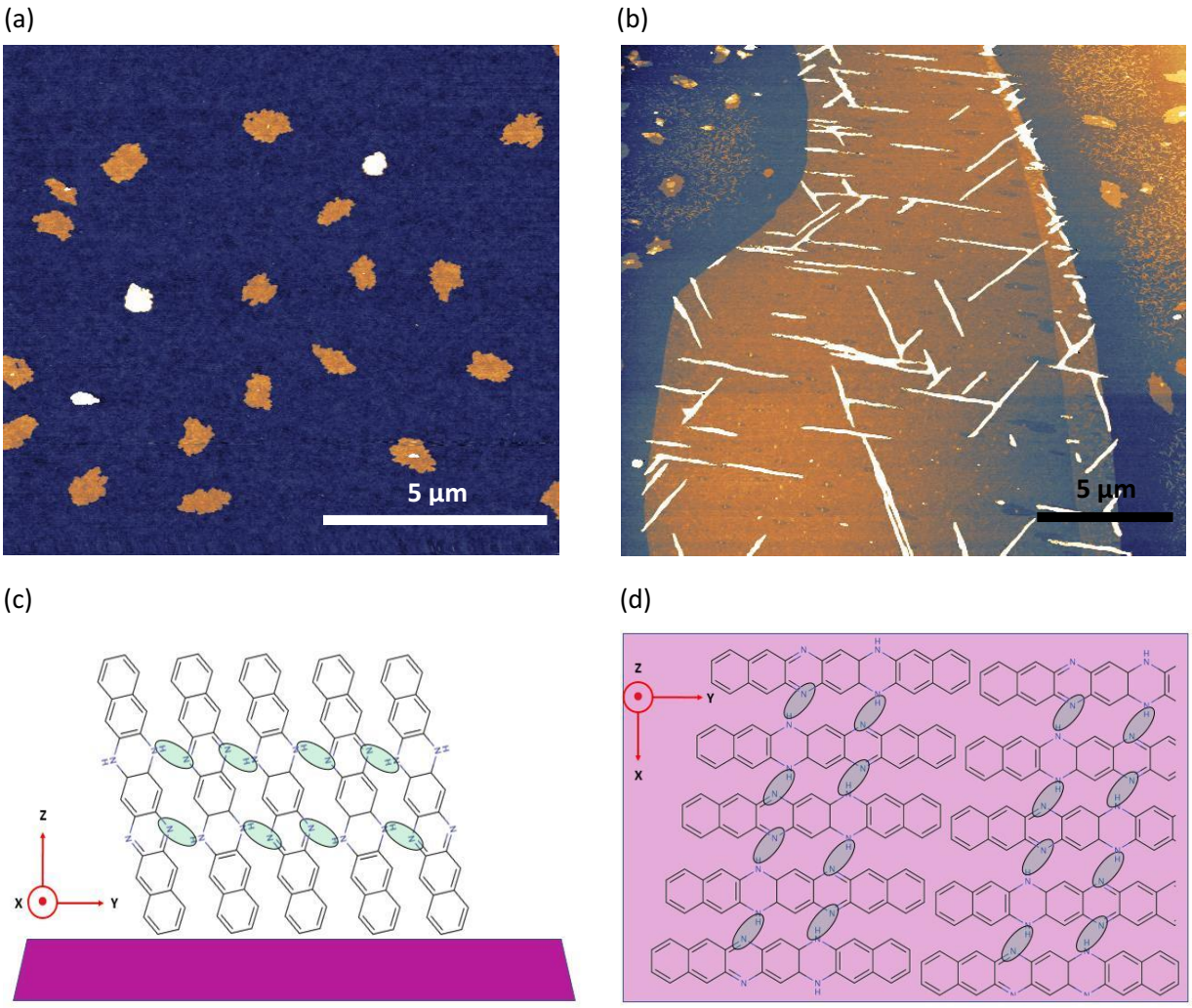

Figure 3: Two different arrangements of DHTA7 molecules on substrates. (a): AFM image of the island-like structures of DHTA7 molecules grown on top of SiO_2. (b): AFM image of the needle-like structures of DHTA7 on top of graphene. (c) upright standing molecules und (d) flat-lying molecules (DFT calculations, courtesy of P. Puschnig, Graz). Z-scale: 4 µm for (a) and 9 µm for (b).

3.2 Exfoliation

Basically, there are two different techniques to create graphene [29]. In the first case, graphene can be isolated from its bulk counterpart – graphite – through cleavage or exfoliation. This can be done either mechanically (scotch tape method) or in liquid usually aided by ultrasonication. The second approach is to form graphene through a chemical reaction from a sp^2 carbon containing precursors. Such examples are chemical vapor deposition, or self-assembly from macromolecules. For the research in this thesis, the method of micromechanical exfoliation has been chosen because of its low-costs and high sample quality. The technique is based on cleavage using the property that the vdW forces between graphene and the surface of substrate are stronger than those between the individual graphene layers.

The procedure for micromechanical exfoliation goes as followed. Starting from a single crystal graphite flake (natural-kish graphite), thin flakes are obtained by repeated peeling between two sides of sticky tape (Nitto Denko Inc.). The film containing many rather thin flakes (in the order of 100 nm thick) iss then deposited on the chosen substrate, and the tape is dissolved in 4-methyl-2-pentanone. Resulting flakes hold to the substrate only by vdW forces. One final step is then applied, where once again the sample is peeled with another tape. This usually leaves only the thinnest flakes attached to the substrate and removes most of the “bulk” graphite flakes that were also deposited during the first step.

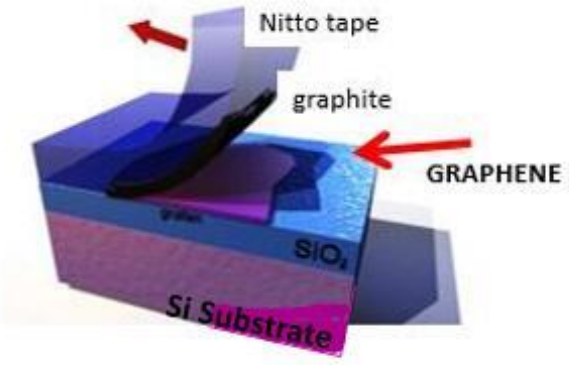

Figure 4: Schematic illustration of the micromechanical exfoliation of graphite [31].

The obtained flakes deviate appreciably in size and thickness, where the sizes range from nanometers to several tens of micrometers for single-layer graphene, depending on the preparation of the used wafer. Although single-layer graphene has an absorption rate of 2%, it is possible to be

observed under a light microscope on SiO_2/Si, due to interference effects [30]. The complexity of this method is basically low, nevertheless the graphene flakes need to be found on the substrate surface which is labor intensive. The quality of the prepared graphene is very high with almost no defects. The basic principle of the micromechanical exfoliation is illustrated in Figure 4. The graphene fabrication using this technique has been done by A. Matković.

3.3 Hot Wall Epitaxy

The precondition of a good analysis on molecule growth is to grow epitaxial layers with high crystalline quality. One of the techniques which has contributed significantly to the preparation of organic thin films with this advantage is the Hot Wall Epitaxy (HWE) [34].

Hot Wall Epitaxy is a vacuum evaporation technique whose main characteristic is the growth of epitaxial layers under conditions closer to the thermodynamic equilibrium compared to other evaporation methods [32] and with a minimum loss of material [33]. A HWE system can be characterized as a semi-closed reactor chamber in which growth of molecules is achieved. Its construction includes a vertically quartz tube (closed at the bottom), which is heated by three separately controllable ovens. The HWE system – and it scheme – which has been employed in this thesis is shown in Figure 5.

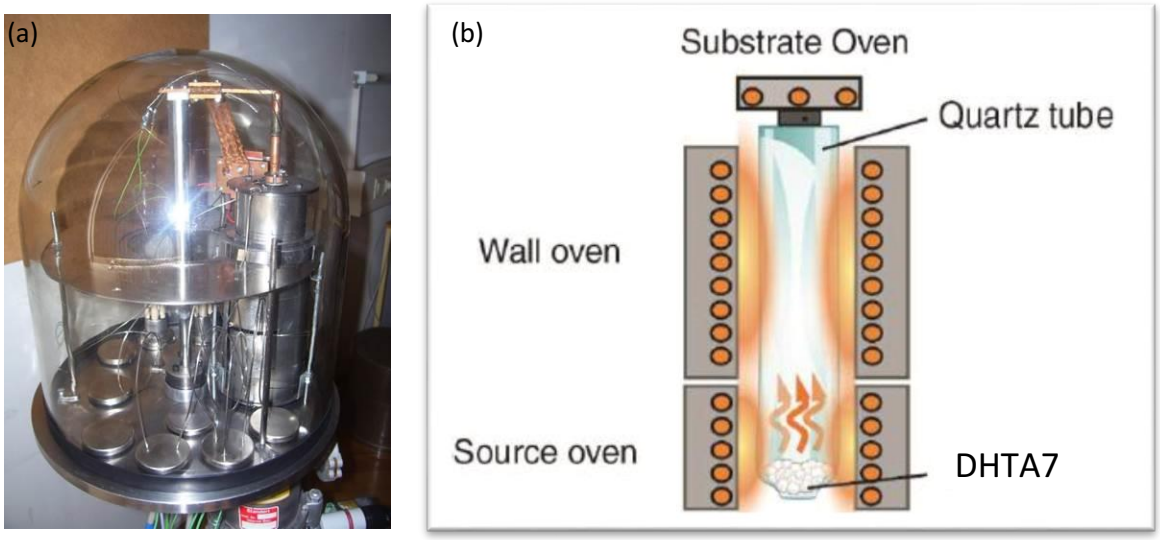

Figure 5: (a) Exterior of the growth chamber in HWE system. (b) Interior schema of the HWE system with quartz tube and three different ovens.

The source material is heated and the growth rate is controlled by the first (source) oven. The hot wall between source and substrate is continuously heated by the second (wall) oven to avoid loss of valuable material. The substrate temperature is controlled by the third one, which allows influence of

the growth process on the substrate surface through the change of the temperature (energy) that the molecules will have upon adsorption. All samples investigated here have been prepared by A. Matković.

3.4 Optical Microscopy

3.4.1 Optical microscopy of graphene flakes

Graphene samples currently used in experiments are fabricated by micromechanical exfoliation of graphite. It is extremely difficult to find small graphene crystallites in the millions of thicker graphitic flakes which appear during the cleavage. In fact, many modern techniques – as: spectroscopic-imaging techniques, atomic-force, scanning-tunneling microscopy, and electron microscopies – that can detect graphene are not able to find graphene easily, because of their extremely low throughput at the required atomic resolution, or are not able to distinguish between atomic monolayers and multi-layer flakes [35]. As an example, Raman microscopy can clearly detect the difference between single- and multi-layer flakes, and can even be used to count layers and estimate defects, strain and doping graphene monolayers [36]. However, it is very hard and time consuming to automate the process to allow for easy search of graphene. In spite its simplicity, the most reliable technique for fast detection of single-layer graphene is still optical microscopy. The main drawback is that high optical contrast of single-layer graphene is achieved only at special substrates that through optical interference increase the contrast of graphene in the visible light range [35].

Because of multiple absorbing events, thin flakes are sufficiently affecting the light path if they are added to an optical path of the bare substrate. This will change their interference color with respect to an empty wafer [1, 35]. If the SiO_2 with a certain thickness (grown on a Si wafer) is used, multiple light reflections within the SiO_2 layer will enhance optical contrast of graphene on top, and even a single-layer can give sufficient contrast to be seen by human eye. This detection technique has promoted a wide use of Si/SiO_2 support for graphene, with specific SiO_2 thicknesses of 300 nm and 90 nm [35, 37].

Figure 6 (a) illustrates one of the graphene flakes used in the thesis, viewed in an optical microscopy under normal, white-light illumination on a Si wafer with the standard 300 nm thickness of SiO_2. In this graphene flake, a few different layers with purple-to-violet color, have been observed. They are monolayer (SLG), bi-layer (BLG), triple-layer (TLG) and few-layer (FLG) which are marked in Figure (a).

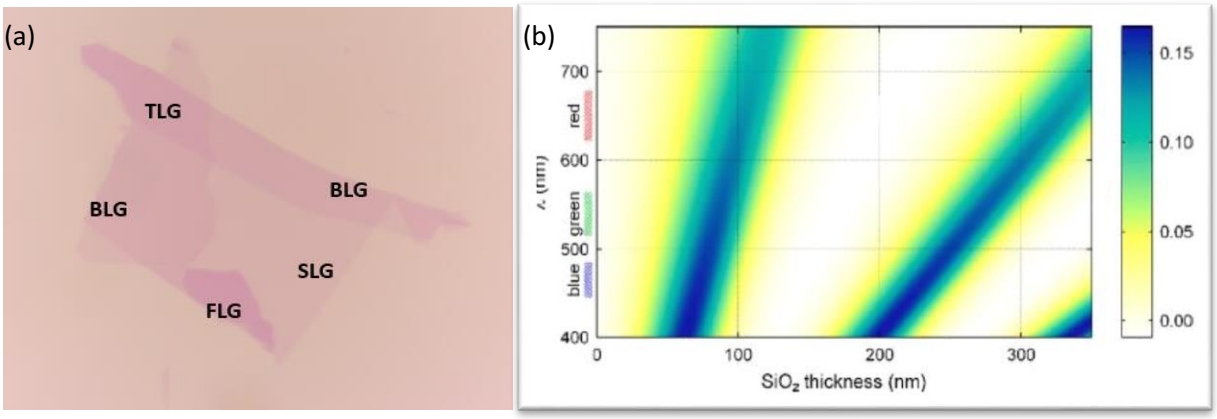

Figure 6: (a) Optical microscopy image at 1000x (120x90 μm^2) magnification show graphene crystallites on 300 nm SiO_2 consisting of a few different layers imaged with white light. (b) Color plot of the contrast as a function of wavelength and SiO_2 thickness [35]. The color scale on the right shows the expected contrast for SLG as a function of SiO_2 thickness.

The dependence of the contrast on the SiO_2 thickness and light wavelength λ can also be investigated. This understanding has allowed people to maximize the contrast and, by using narrow-band filters, to find graphene on practically any substrate. To illustrate the selection for the thickness of the oxide layer of SiO_2/Si wafers, Figure 6 (b) shows a contrast plot (between SiO_2/Si and graphene/SiO_2/Si) as a function of SiO_2 thickness and wavelength of light in the visible range [35].

3.4.2 Enhanced optical contrast of DHTA7 needles

"The optical systems contained in modern microscopes may be capable of producing high resolution images at high magnifications, but such a capability is worthless without sufficient contrast in the image. Contrast is not an inherent property of the sample, but is dependent upon interaction of the sample with light and the efficiency of the optical system. Control of image contrast in the microscope optical system is dependent upon several factors. The most critical to the optical system are the field and the condenser aperture diaphragm settings" [38]. High-resolution optical microscopy of organic molecules typically suffers from a lack of contrast, especially when long needle structures are formed. It renders these needle structures not sharp or nearly invisible which causes difficulties for the analysis (Figure 7 a). Using the full aperture of the microscope objective, also hinders the contrast of the molecules due to saturation of the detector at the edges which are not of interest in most cases. To adjust contrast, some specialized contrast-enhancing accessories such as filters were employed within the software of the optical microscope (Zeiss Axio Lab1). Then, the light around the sample was focused through a change of aperture size. The enhanced effect of needle

structures on graphene by optical microscopy is illustrated in Figure 7 b. Optical microscopy analysis was performed together with A. Matković.

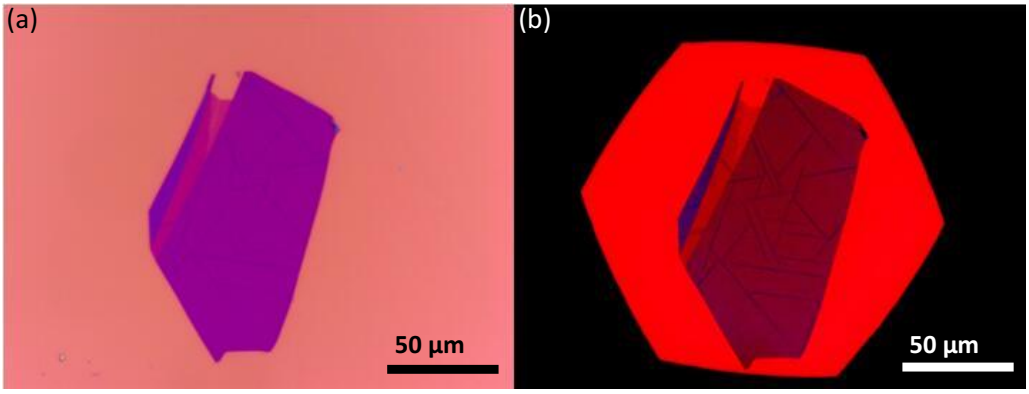

Figure 7: Optical microscopy images at 500x magnification (240x120 µm^2) of a FLG graphene flake with DHTA7 needles. (a) "As seen by the eye" image without enhancement of contrast, (b) image with enhanced optical contrast of DHTA7 needles.

3.5 Atomic Force Microscopy

In order to resolve nanometer scale features in the sample topography, Atomic Force Microscopy as a type of scanning probe microscopy (SPM) was chosen [39]. The information is gathered by "feeling" or "touching" the surface with a mechanical probe. AFM can be used for three major applications as force measurement, imaging and manipulation. In force measurements, the forces between the probe and the sample are measured and can applied to perform force spectroscopy. In manipulation, the forces between tip and sample are used to change the properties of the sample in a controlled way. In the case of imaging, the forces that the cantilever exhibit due to the interaction with the sample is used to image the morphology of the sample's surface. Commonly, an electronic feedback is employed in such way that for every measured spot the force is kept constant by changing the height of the probe. That way by recording the height change of the probe, the surface of the sample is reconstructed [40]. For this thesis, only the imaging capability of the AFM was used. During the measurement, a deflection of the cantilever is caused by the forces between the sample and the tip. It can be measured by a laser which is directed to the end of the cantilever and reflected from them to a split photodiode. Piezoelectric elements that facilitate tiny but accurate and precise movements on command enable very precise scanning. With the topographical image, further information such as stiffness and electrical properties can also be obtained [41]. The schematic principle of the AFM setup is illustrated in Figure 8.

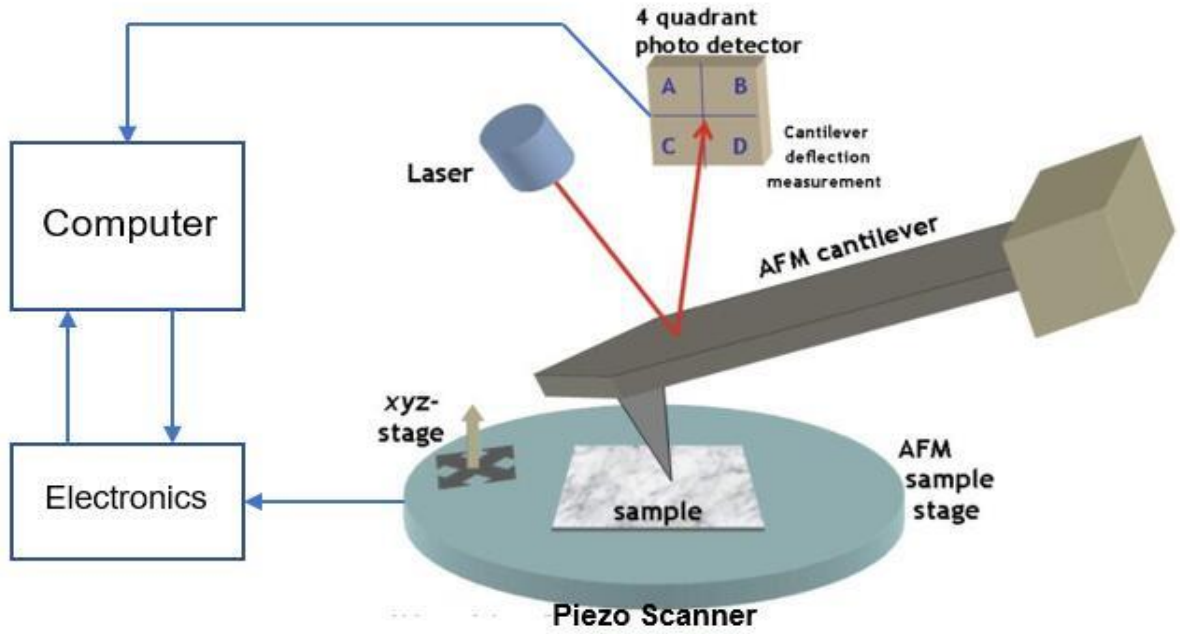

Figure 8: Schematic principle of the AFM setup [40]

In general, possible imaging modes are divided into static (also called “contact”) modes and a variety of dynamic (“non-contact” or “tapping”) modes where the cantilever is oscillating at a given frequency. For the research in this thesis, tapping mode is the method of choice. In this mode, the cantilever is oscillating near its resonance frequency. The oscillation amplitude is used as a regulating signal to scan the surface. Although the tip touches the sample, even with higher peak forces than that during contact mode, tapping mode usually reduces the damage done to the tip or surface compared to the amount done in contact mode. This can be explained by the short duration of the applied force and the significantly lower lateral forces. This mode is generally used for measurements under ambient conditions.

Characterization of the graphene sample before and after deposition of DHTA7 molecules is performed with help of a Nanoscope III Multimode atomic force microscopy from Digital Instruments. Olympus AC160 probes were used. These probes are designed for non-contact (tapping mode) measurements, with spring constants typically between 20 Nm to 30 Nm, and apex diameter between 4 nm and 10 nm. For the research on morphology of deposited DHTA7 molecules on top of graphene and SiO2 in this thesis, the primary advantage of the employed AFM is a very accurate scanning of rather small surface area on the sample (usually about 5x5 µm2 area). The instrument can afford a maximum scanning area of about 90 x 90 µm2.

Figure 9: Photography of the Multimode AFM used in this thesis

Since the cantilever operates in tapping mode, it is no longer continuously in contact with the surface, both tip and sample degradations is minimized [42]. This is very important for this thesis, since organic molecules – as DHTA7 – form fragile nanostructures and could not be measured in contact mode without severe damage to the sample.

3.6 AFM data analysis using Gwyddion software

Gwyddion is a modular software program for SPM data visualization and analysis [43]. The version 2.46 of this software has been used within this research. In Figure 10, the image processing is illustrated. The original image from AFM is shown in Figure 10(a). Figure 10(b) shows the same image as in Figure 10(a) after applying "Level data by mean plane subtraction". The mean plane is computed from all the image points and is subtracted from the raw SPM data (Figure 10(a)). The next applied function attempts to deal with artifacts that may occur in a scan line direction. Figure 10(c) shows the results after applying the following steps: *Data Process → Correct Data → Step Line Correction*. The last procedure that is commonly applied to all the AFM topography images "Level data by fitting a plane through three points" is shown in Figure 10(d). The "Three Point Leveling" tool

can be used for proper leveling of surface structures, as steps, terraces, or any similar structures that may have flat areas at the different height levels. It is needed to simply select three points in the image that should be at the same level, then the plane passing through those three points is subtracted from the image.

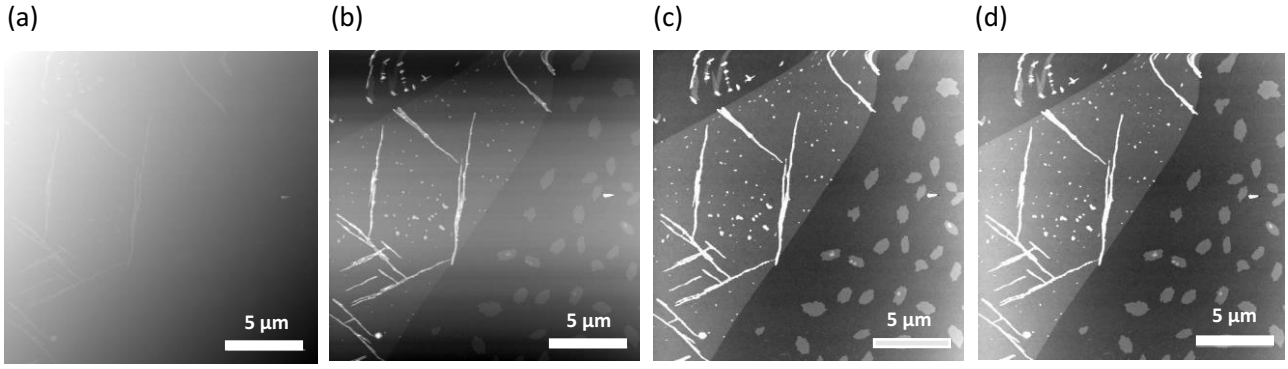

Figure 10: 20x20 µm^2 AFM images of DHTA7 on graphene and SiO_2, (a) Raw image, (b) after mean plane subtraction, (c) after step line correction, and (d) after three-point-plane correction, z scales 300 nm (a), 35 nm (b), 10 nm (c,d).

3.6.1 Surface coverage estimation of DHTA7 islands on SiO_2

Sometimes, adatoms or molecules are more strongly bound to each other than to the substrate: Direct nucleation of small clusters on the surface, which then grow into 3D islands of the condensed phase. This so-called island growth mode of DHTA7 is usually found on SiO_2 surfaces of the sample. The following Figure 11(a) has been chosen here to show the typical morphology of DHTA7 molecules on SiO_2. The height of DHTA7 in form of islands can be measured using "Extracts profiles" function. The height profile is then shown in Figure 11(b), in which an island height of about 1.9 nm was observed. This is in a good agreement with the expected height of the up-right standing DHTA7 molecules.

How to estimate the surface coverage of these molecules on SiO_2 is introduced by the following steps: The grains are marked by height threshold and then the volume related properties can be calculated using several different functions. In this study, the height threshold function of Gwyddion was used as the most appropriate method to differentiate DHTA7 islands from the substrate. This function can be accessed within Gwyddion through: *Data Process* →Grains → Marked by Threshold. Height, slope, or curvature thresholding is implemented within this module. The effect after using this function is demonstrated in Figure 11(c).

For the total number of marked grains, their total projected area can be calculated by a function which is accessed as *Data Process* → *Grains* → *Statistics.* With the obtained data, the volume of DHTA7 molecules per unit area on SiO_2 can be calculated.

(a)

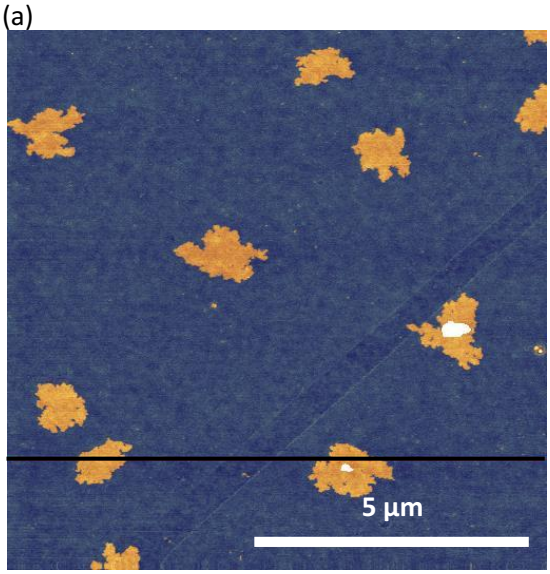

(c)

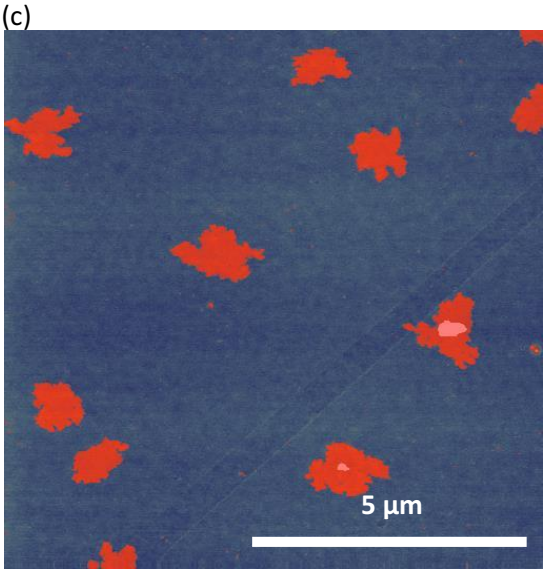

(b)

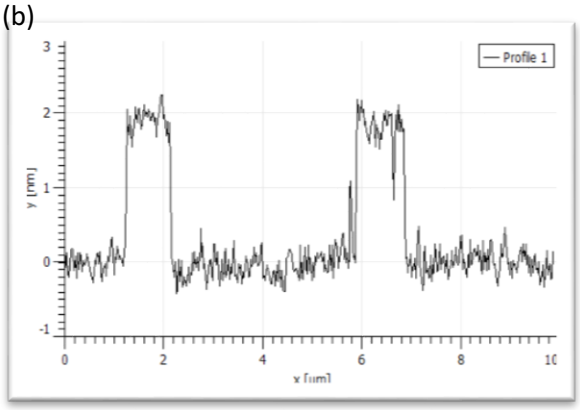

Number of Grains:	94
Total projected area (abs.):	6.678 µm^2
Total projected area (rel.):	6.68 %
Mean grain area:	71 x 10^{-15} m^2
Mean grain size:	113.3 nm
Total grain volume (laplacian):	14 x 10^{-21} m^3

Figure 11: 10 x 10 µm^2 AFM images, z scale 5 nm, in which the application of grain analysis and all volume related properties on the surface of SiO_2 is demonstrated. The black line in (a) indicates a height profile shown in (b). The red marked masks in (c) represent the area which is used to calculate the volume related properties (shown in the table below (c)).

3.6.2 Needle length and orientation analysis

In comparison to the analysis of islands, a different procedure is used for needle analysis on the graphene substrate as is illustrated in Figure 12. The selection of needles can be accessed as *Tools* → *Measure distance and direction between points* which is shown in Figure 12(a). The measurement of horizontal and vertical distance, and angle between points in the data field is enabled by this tool. In addition, the difference of data values between points can be displayed.

It is known that the Fourier transform decomposes a signal into its harmonic components and is therefore useful while studying repeating patterns and directions present in the SPM data. Two-dimensional Fourier transform can be accessed using *Data Process* → *Integral Transforms* → *2D FFT* in which the Fast Fourier Transform (FFT) is implemented. The 2D FFT module provides several

types of output. The effect of “Modulus” type, corresponding to all the selected data from Figure 12(a), is presented in Figure 12(b).

(a) (b) (c)

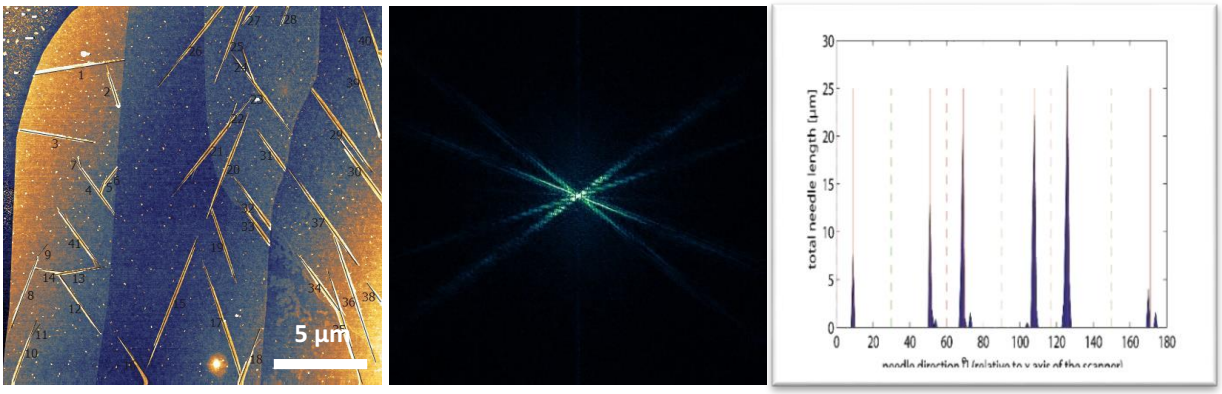

Figure 12: (a) 20 x 20 µm^2 AFM image of DHTA7 molecules grown on top of a graphene flake, with each individual needle selected, z scale: 4 nm, (b) 2D FFT image of (a). (c) Histogram of accumulated needle length as a function of growth directions; results of angle analysis from selected needles within (a).

To determine the angular distribution on top of the graphene substrate, also a histogram of accumulated needle length as a function of growth directions was used. The data received from the needle selection (manually selected each needle) can be used to obtain a histogram which is shown in Figure 12(c). The step for the histogram was kept fixed to 1° and each needle is checked if its angle is within ± 0.5° from the current histogram step. If so, the length of that needle was added to the current histogram point, and the needle taken out from consideration. The same procedure was repeated for every histogram point, starting from 0° to 180°. The x-axis displays the DHTA7 needle growth direction and the y-axis shows the total length of needles in corresponding direction. The accuracy (a histogram column) was kept fixed to 1° for all analyzed samples. Compared to the 2D FFT analysis, this procedure is rather time consuming but yields immediately real-space information.

4. Results and data analysis

The surface morphologies of all the samples are observed by AFM. It is noticed that the deposition temperature T_D has a strong influence on the surface structures of the films. In order to estimate the growth of DHTA7 molecules on top of graphene and SiO_2, a temperature interval of T_D from 313 K to 393 K has been chosen.

4.1 Growth morphologies of DHTA7 on SiO_2

Which growth mode is favored during epitaxial growth depends on the interfacial energy and the degree of lattice mismatch. With the results of this temperature series, it is demonstrated that DHTA7 molecules could be grown in either Frank–van der Merwe or Stranski–Krastanov mode on top of SiO_2. To determine the exact mode would require thicker structures to be grown. The overwhelming feature of grown DHTA7 on SiO_2 is observed as island-like structures. After analysis by Gwyydion, a temperature series has been found to show the dependence of growth morphology on different T_D which is displayed in Figure 13 (a-e).

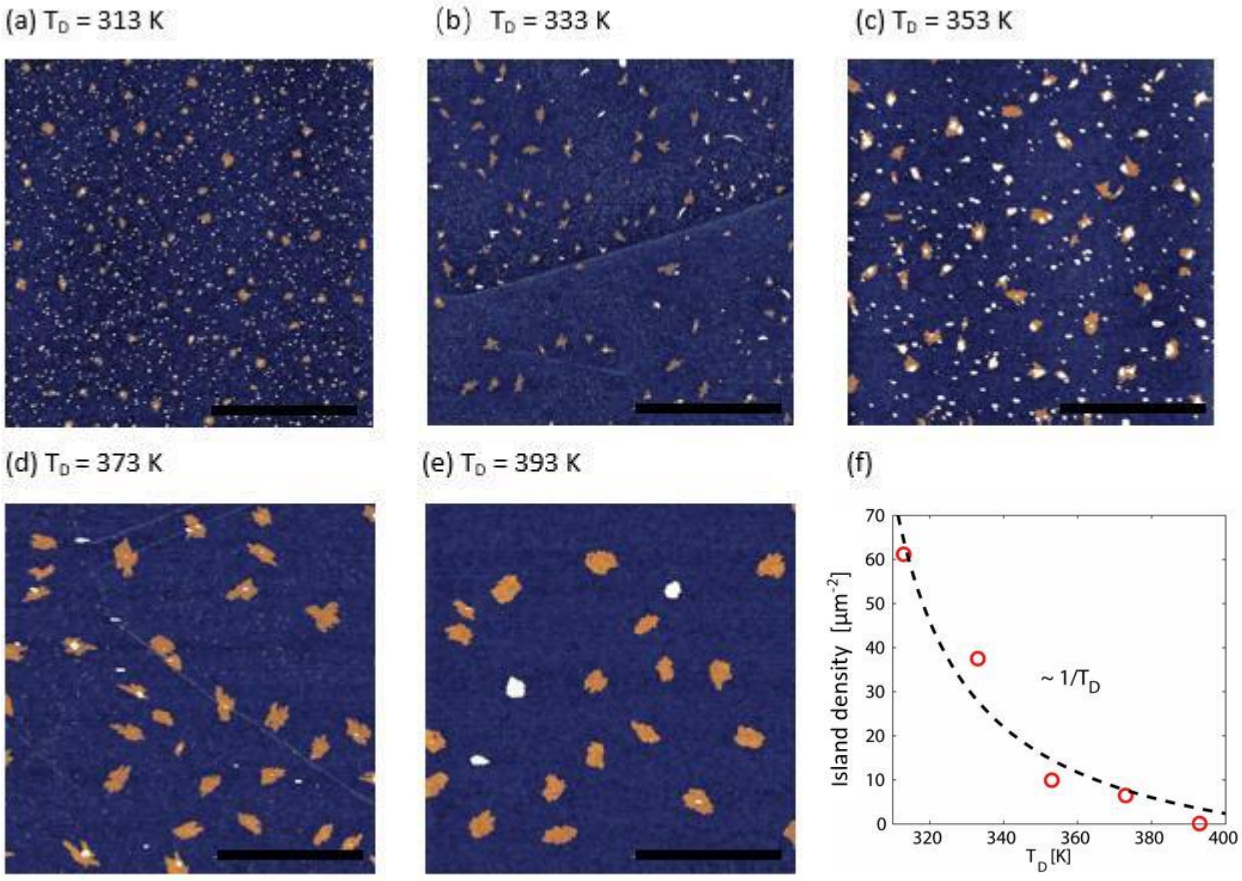

Figure 13: (a-e) 10 x 10 µm^2 AFM images of grown DHTA7 molecules on SiO_2 in form of island structures which have dependence on a series T_D. Lateral scale bars: 4 µm, z scales: 5 µm. (f) Number of island nucleation points per µm^2 as a function of T_D.

For better understanding of the nucleation of islands, a definition “jump rate” of a surface molecule from a lattice site should be introduced: $P = D / L^2$. (P: jump rate, D: diffusion constant, L: jump length). It is also known that the diffusion constant D behaves as a function of deposition temperature T_D: $D = D_0 \exp[-E_A/(kT)]$. (D_0: diffusion constant, E_A: activation energy, k: Boltzmann´s constant). The DHTA7 molecules can´t jump onto the top of existing islands so it leads to a diffusion of the molecules only along the edge of them.

In this temperature series, some properties of grown islands have also been revealed. The island-like structures are always grown with the same height, even if the T_D changes. Number of islands decreases but they grow larger with increase of T_D, and are less dendritic. The number of small needle- and dot-like structures reduces with increasing T_D.

4.1.1 Terraced island growth of DHTA7 on SiO_2

A phenomenon that lying-down molecules forming needles versus upright standing molecules grown on top of SiO_2 at the same time is revealed in Figure 14 (a). The island structures which are composed of almost upright standing molecules can be noticed well here. Mound formation due to a so-called Ehrlich-Schwoebel barrier (ESB) [44] can also be found. This is because DHTA7 molecules sometimes cannot overcome the extra barrier across step edges. They are reflected at the step edge and form with other molecules a new island on top of the existing one. Terraced growth mounds are therefore formed instead of layer-by-layer growth [44].

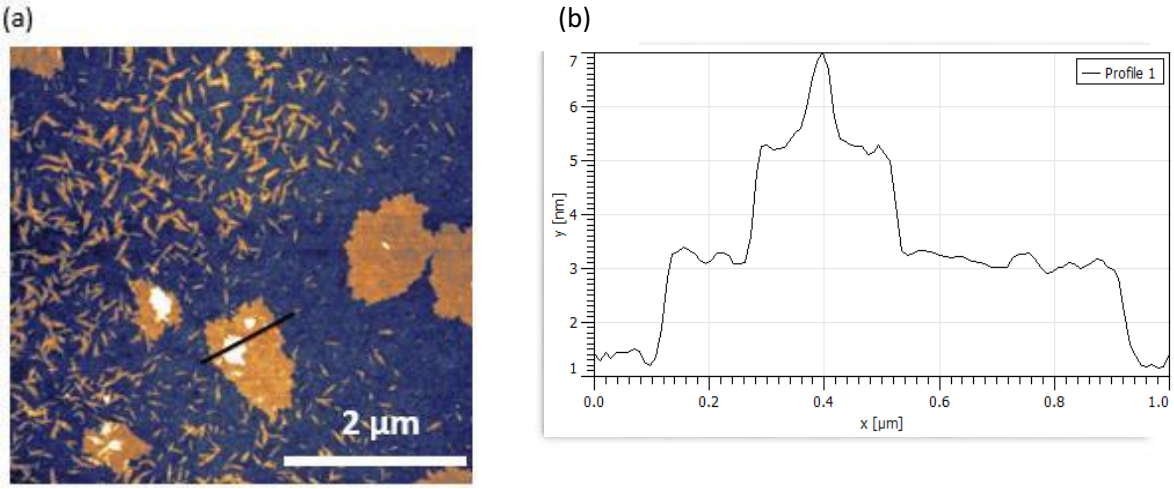

Figure 14: (a) 5 x 5 μm^2 AFM image of grown DHTA7 on SiO_2 with needle and island-like structures at T_D = 353 K, z-scale: 5 nm. (b) Height cross-section of a terraced island marked by the black line in (a).

From the height profile presented in Figure 14 (b), a three-layer grown island structure has been displayed. It is noticed that each layer here exhibits a height of about 2 nm, which corresponds well to the length of one upright standing DHTA7 molecule.

4.2 Growth morphologies of DHTA7 on graphene

Previously reported results for rod-like, aromatic, organic molecules on graphite and graphene surfaces indicate that molecules tend to adsorb face-on with the molecular long axis parallel to high symmetry direction of the substrate that best matches the molecular structure (zigzag for acenes and armchair for phenylenes) [45, 46]. However, direction of needle growth is perpendicular to the long molecular axis [46]. Moreover, there is in fact a little deviation from the direction that is opposite from the one in which the molecule adsorbs [45, 46]. In order to focus on these needle-like structures of DHTA7 molecules on graphene, several investigations according to growth morphology, needle length, needle directions and volume ratio have been performed into this thesis.

The growth of DHTA7 molecules on graphene shows an abnormal dependence on T_D, as observed in this temperature series and presented in Figure 15. In general, a higher deposition temperature is needed to form long needle-like structures. While at 313 K only randomly oriented short crystallites are observed in Figure 15(a), films grown at 333 K exhibit needle-like crystallites of up to 20 µm in length (Figure 15(b)). The deposition of 333 K leads not only to extremely long needles but also an orderly growth. With increasing T_D, the length of needle-like structures decreases again and the growth of deposited molecules changes into dot-like, irregular structures (Figure 15(c-e)).

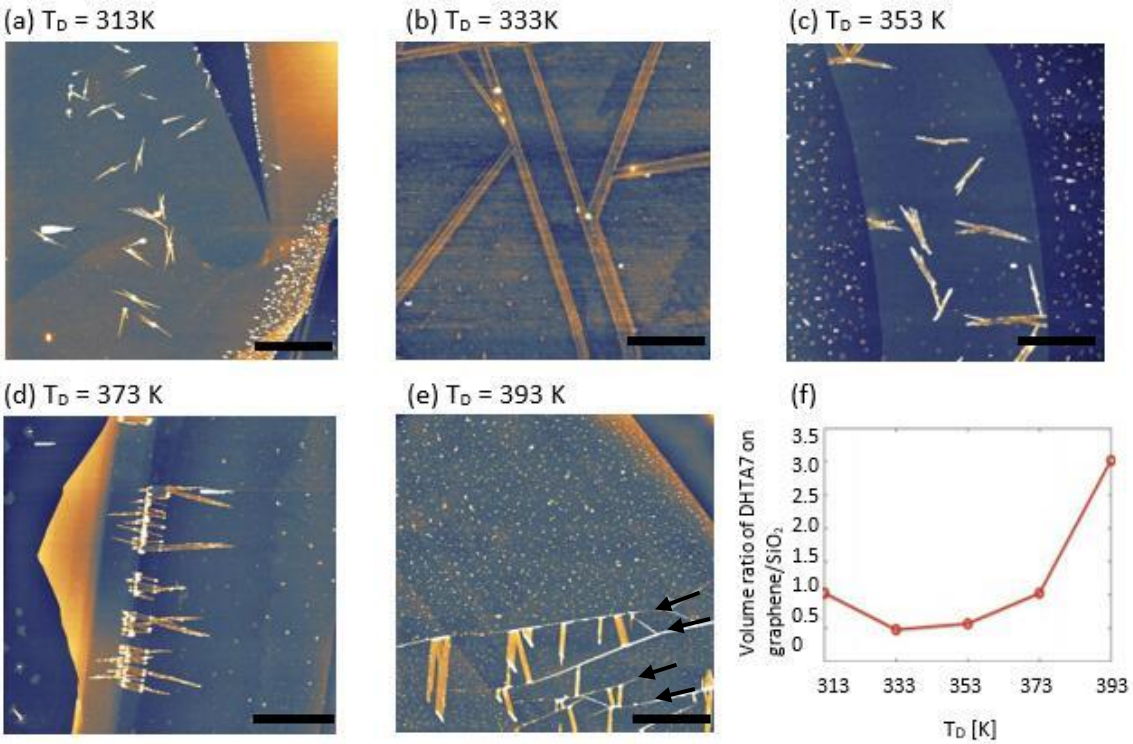

Figure 15: 20 x 20 µm^2 AFM images of DHTA7 molecules on single- and few- layer graphene in form of needle-like structure for different T_D from 313 K to 393 K. Lateral scale bars: 5 µm, z scales: 10 nm (a, c, e), 5nm (b), 15 nm (d). Black arrows in (e) indicate wrinkles in graphene flake. (f) The volume ratio of DHTA7 on graphene/SiO_2 as a dependence of T_D.

The high value of the volume ratio of DHTA7 on graphene/SiO_2 at a T_D of 393 K shown in figure 15 (f), has revealed that the volume within the needles is not increasing at higher T_D, but the dot-like structures significantly increase. This phenomenon is different in comparison to the growth morphology on SiO_2 which has already been investigated in the previous chapter. The dot-like structures on SiO_2 decrease with increasing T_D and disappear at 373-393 K (Figure 13 (d) and (e)), but they exhibit a significant increase on graphene at these temperatures.

Figure 16 reveals the magnified area of one needle-like structure formed at 353 K which is shown in Figure 15 (c). The irregular growth of needle is well observed. The structures formed are most likely due to contaminant initiated nucleation in the middle of the branching needles.

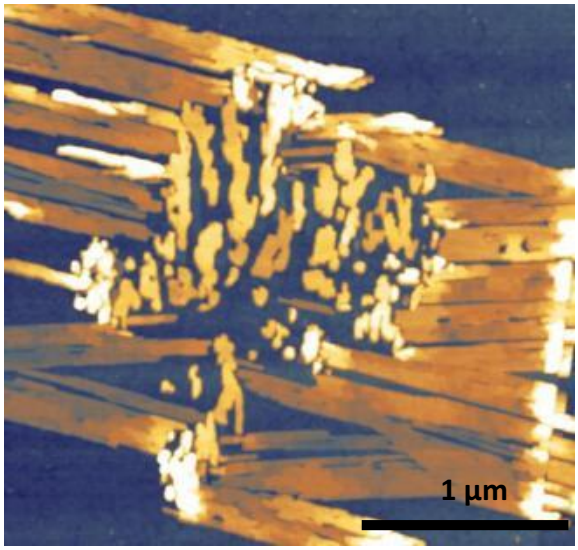

Figure 16: 2.5 x 2.5 µm^2 AFM image of DHTA7 molecules deposited on graphene at 353 K with branching needle-like structure, z scale: 10 nm.

The deposition at high substrate temperature leads to a change of growth of DHTA7 molecules on graphene which is observed in Figure 15 (d) and (e). Needle-like structures were not found nucleating in the middle of the graphene flake. They prefer to nucleate either at the edges of graphene layers (Figure 15 (d)) or along the wrinkles which are sometimes forming in the fabrication process (black arrows in Figure 15 (e)).

4.3 Size analysis of DHTA7 needle-like crystallites

For the analysis of needle growth, the average length of DHTA7 needles on graphene and graphite flakes was evaluated. Figure 17 (a) shows an optical image (1000x) of the DHTA7 in form of needle structures, grown on bulk graphite (T_D = 333K). In order to get the average length of the needles, the length of each needle visible within the given optical or AFM image was considered. A histogram of

needle length, corresponding to the structure shown in Figure 17(b) is presented in Figure 17(a). A statistic of numbers corresponds to different length of all needles is then obtained from the position of the main peak in the histogram, as indicated in Figure 17 (a). Figure 17 (c-f) shows similar data for two more deposition temperatures, demonstrating that needles indeed grow much shorter as T_D is increased beyond 333 K.

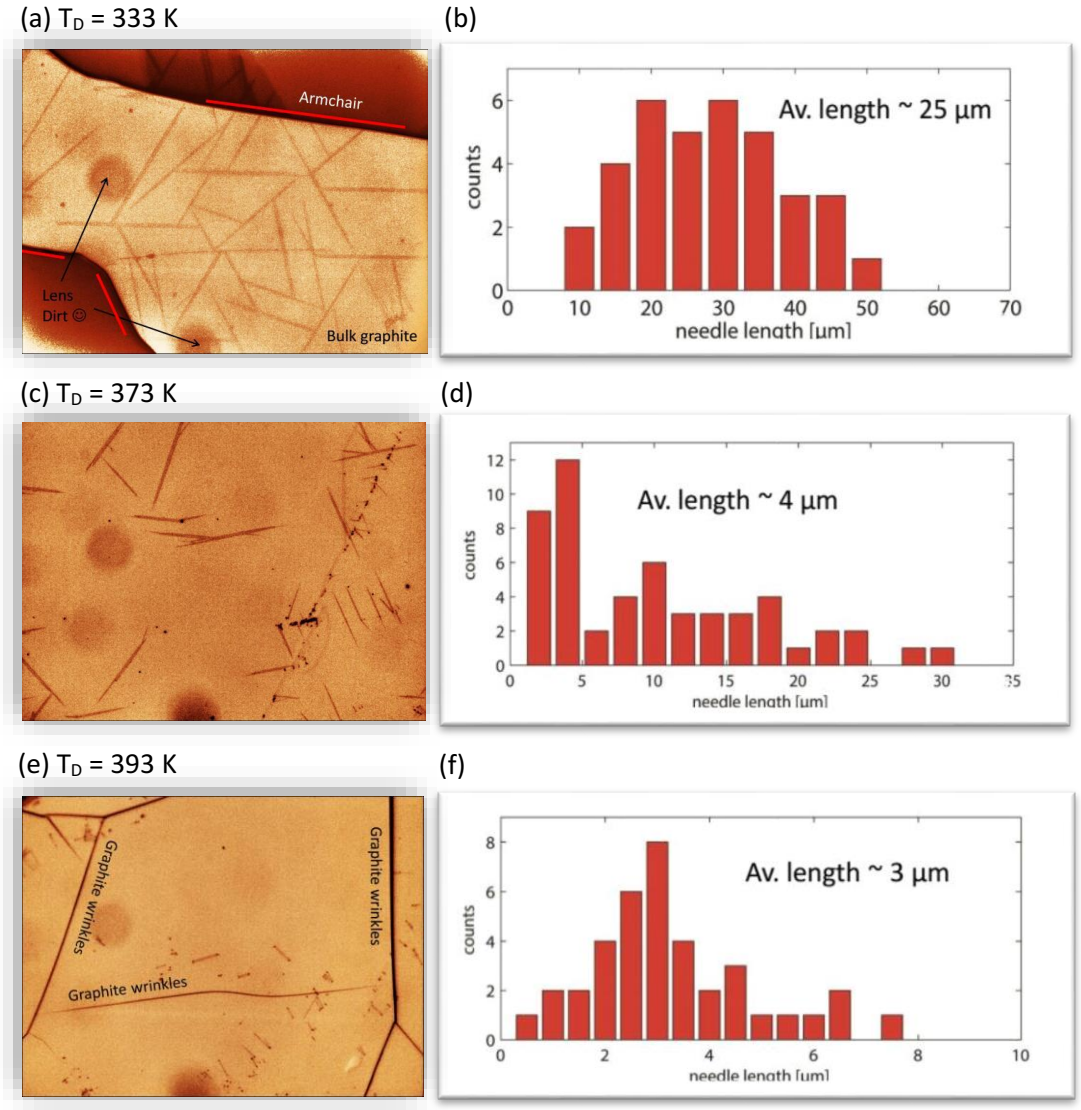

Figure 17: (a,c,e) Optical microscopy images at 1000x magnification (120x 90 µm^2 with enhanced optical contrast through image filtering) of bulk graphite flakes with DHTA7 needles. (b,d,f) Histograms of needle length also indicating obtained average values.

In order to investigate the average DHTA7 needle length on top of graphite flakes, the tools "Distance" and "Extract profiles" provided by the software Gwyddion which was already mentioned in chapter 3.6, was used. Figure 18 shows the statistic results of average needle length with different deposition temperatures. At low temperature (313 K), DHTA7 molecules form very short needles with an average value of below 2 µm, for this reason it was not possible to analyze optical images of

these very small crystallites and only AFM data was considered. At a little higher T_D around 333 K, the average length is increased to a high value of 25 µm. At higher temperatures (353-393 K), the length of the needles again decreases as seen in Figure 18.

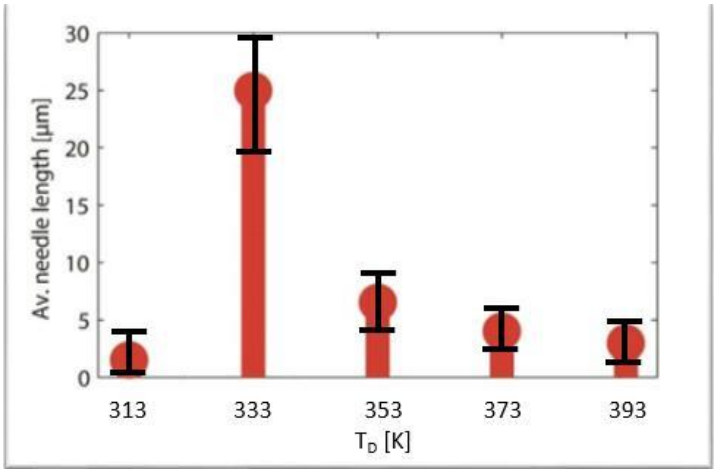

Figure 18: Average needle length of DHTA7 on top of bulk graphite flakes as a function of T_D. A significantly increased value of the average length is well observed at T_D = 333 K.

4.4 Orientation analysis of DHTA7 needle-like crystallites

For further analysis of the needle growth and the epitaxial relation between the molecules and the substrate, the angular distribution of DHTA7 needle on graphene flakes was also evaluated. This can be obtained according to the same method that has already been mentioned in chapter 3.6.2.

Figure 19 summarizes the growth behavior of DHTA7 needles grown on single- and few-layer graphene flakes with a series temperature from 313 K to 393 K. In order to obtain the angular distribution of the needles, the direction of each needle was manually analyzed with respect to the x-axis of the scanner, and measured counter-clock-wise. The analysis of the growth directions was independently done also by considering the two-dimensional Fourier Transform (2D-FFT) of the morphology images, with results presented in the middle column of Figure 19. The total length of all needles according to their respective directions, corresponding to the needle structures shown in the left column of Figure (19), is measured in the right columns of the Figure 19. Also, the directions of the sharp edges of the graphene flakes are marked by dashed red and green lines. In these histograms, it can be seen that DHTA7 needles structures tend to follow primarily one of these directions, namely the ones marked by dashed-red lines (armchair – also will be discussed in chapters 4.5 and 4.6). Interestingly, the amount of DHTA7 needles grown exactly in the “armchair” direction is almost zero. Instead, a deviation of about ± 9° to “armchair”, indicated by the solid-red lines, is revealed.

AFM morphology 2D FFT Accumulated needle length

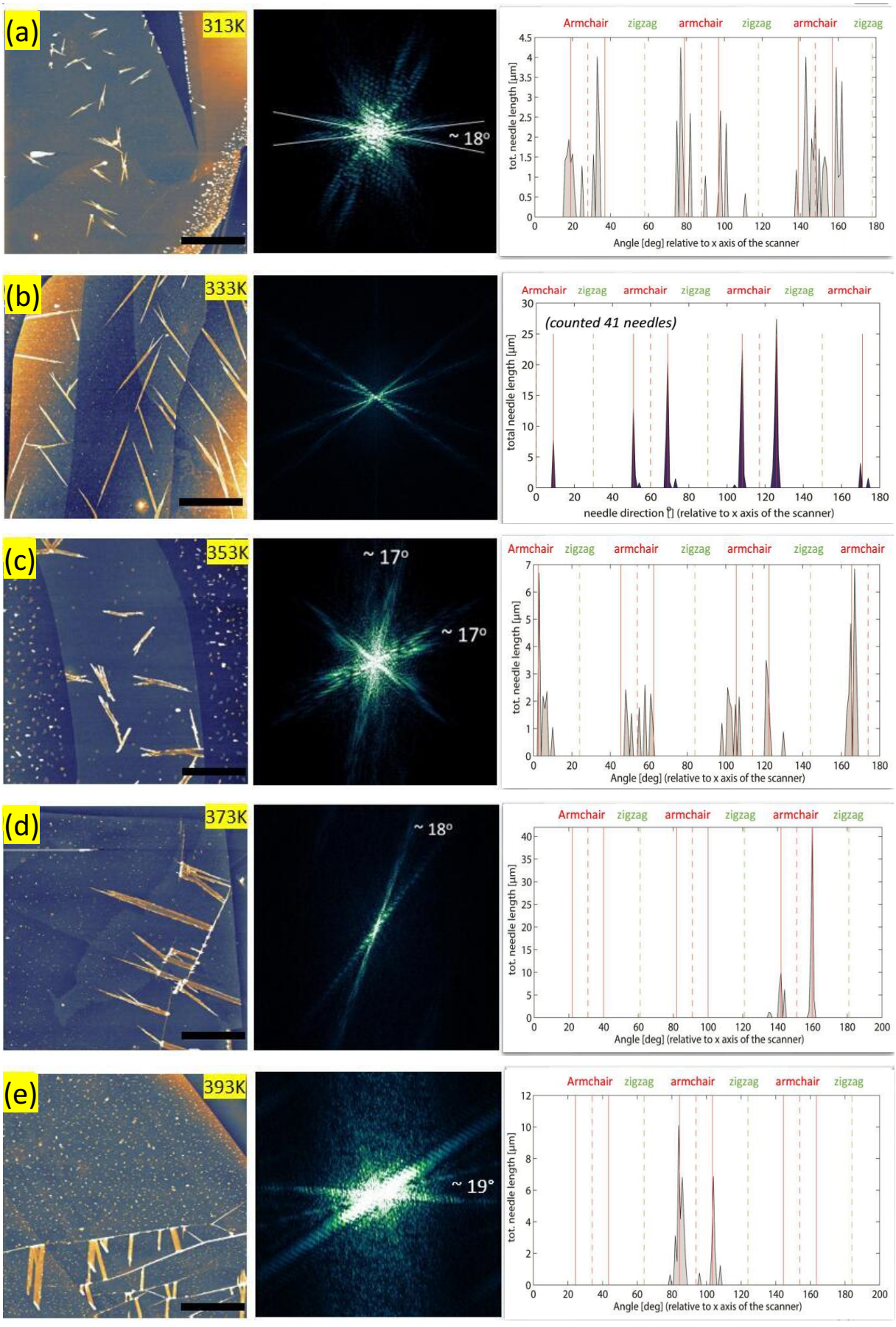

Figure 19: Needle orientation analysis for (a) 313 K, (b) 333 K, (c) 353 K, (d) 373 K, and (e) 393 K. Left column: 20 x 20 μm^2 AFM images of DHTA7 molecules on single- and few- layer graphene in form of needles-like structures. Lateral scale bars: 5 µm, z scales: 10nm (a) (c) (d) and (e), 4nm (b). Middle column: Corresponding 2D FFT diagrams. Right column: Total needle length according to respective direction with respect to the x-axis of the AFM scanner, with ± 0.5° accuracy. The x-axis in subfigures shows the DHTA7 needle growth direction (taken counter-clock-wise from the x-axis of the scanner of the AFM topography image, which is considered as 0°), while the y-axis displays the total length of DHTA7 needles in the given direction. Dashed red and green lines indicate armchair and zigzag directions of the graphene flake respectively. Solid red lines represent ± 9° splitting from armchair directions of graphene flakes.

It is easily noticed that because of the randomly oriented short crystallites at T_D = 313K, DHTA7 needles tend to follow "armchair" directions forming six peaks separated by a certain degree. Most of the angular distributions conform the deviation of about ± 9° (Figure 19 a, right). This needle direction splitting becomes much more obvious when T_D is increased to 333K, the orderly growth of needle-like structures leads to a homogeneous angular distribution corresponding to deviation of ± 9° around these "armchair" directions which is shown in Figure 19 (b). With increasing T_D, irregular structures due to contaminants-initiated nucleation broaden the distribution again (Figure 19 c). At even higher T_D (373 K and 393 K), because of the affinity of the needles to nucleate at wrinkles and step edges, the angular distribution shows peaks only along two directions according to the deviation from "armchair", giving again sharp growth directions both in FFT images (Figure 19 d, e middle) and in the histograms (Figure 19 d, e right). Although the deposition temperature clearly affects the preferred nucleation sites for the needles, their degree of uniformity, and lengths, still the relative orientation remains the same in the entire range considered. This clearly shows that the needles always have the same epitaxial relation with the substrate, splitting from a high-symmetry direction (armchair) of graphene by about ± 9°.

4.4.1 Estimates of the preferred growth directions uncertainty from 2D FFT images

Figure 20 illustrates the estimation of the error in the deviation value from 2D FFT analysis of the AFM images. The deviation of about ± 9° from the high symmetry direction in graphene is denoted by the white-solid line in FFT image (Figure 19 middle column). Actually, this angle measured between both bright lines (about 18°) in FFT image has an approximate value. It should be noticed that the bright lines in FFT images are not thin and uniform, which cause uncertainty of the determined angles. The uncertainty was estimated from the "full width at half maximum" (FWHM) of a cross-

section of each line in the 2D FFT images for every sample (at different T_D). The method used to estimate the uncertainty of the growth directions is explained on the example of a sample grown at T_D = 333 K.

(a) (b)

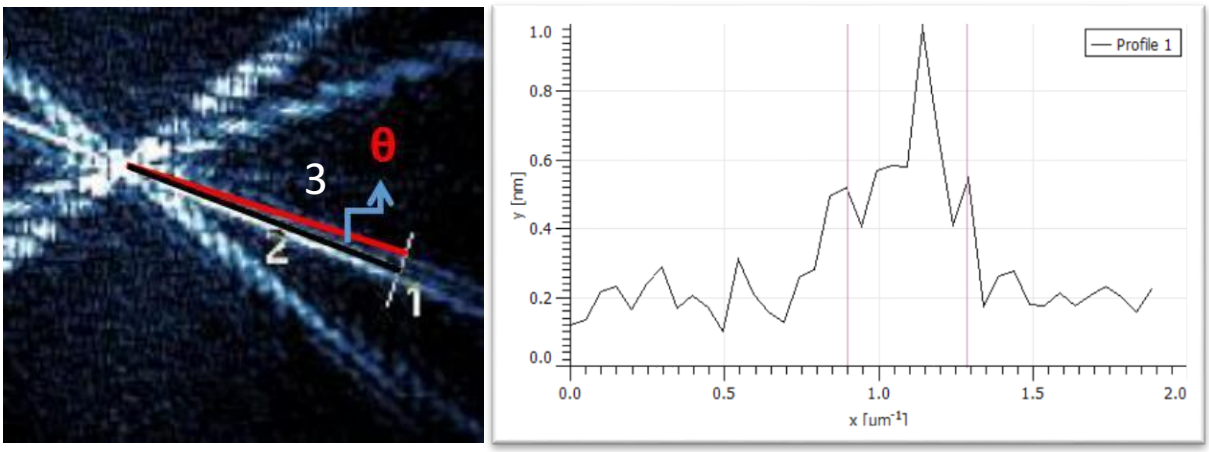

Figure 20 (a) magnified area of a 2D FFT image shown in Figure 19 middle column next to (2a). (b) Cross–section of the "Line 1" from (a). Line number2 starts from the center of the 2D FFT image and follows the highest intensity of the lines visible in the image. Line number 1 is perpendicular to line 2, and intersects line 2 sufficiently far from the center of the image to avoid noise. Line 3 connects the center of the 2D FFT image and the left FWHM point in line 1.

Figure 20 (a) shows the magnified area of one bright-line direction which is shown in Figure 19 (2b). The Width of this bright line can be measured by considering the cross-section of "Line 1" which is perpendicular to "Line 2", as shown in (b). The length between two solid vertical lines which is shown in (b), corresponds to the FWHM of that particular needle growth direction, indicated by a solid black line (Line 2) in (a). The distance from middle point to "Line 1" is measured by black "Line 2". Angle formed by black and red lines in (a) is defined as "θ", and represents the uncertainty of the measured needle growth direction. Then the angle variation can be treated as a calculation problem in a triangle consisting of a red "Line 3", black "Line 2" and a half value of width measured by white "Line 1".

The values of several angle θ can be calculated using trigonometric function and the angle variation of needle structures distribution is an average of them. Figure 21 shows the comparison of these average values as a function of T_D. It reveals that the smallest uncertainty of needle growth direction occurs at a deposition temperature of 333K and 373K, and in all cases the uncertainty of the measured angles for the needle growth direction is several times smaller than the splitting angle for the two mirrored growth directions.

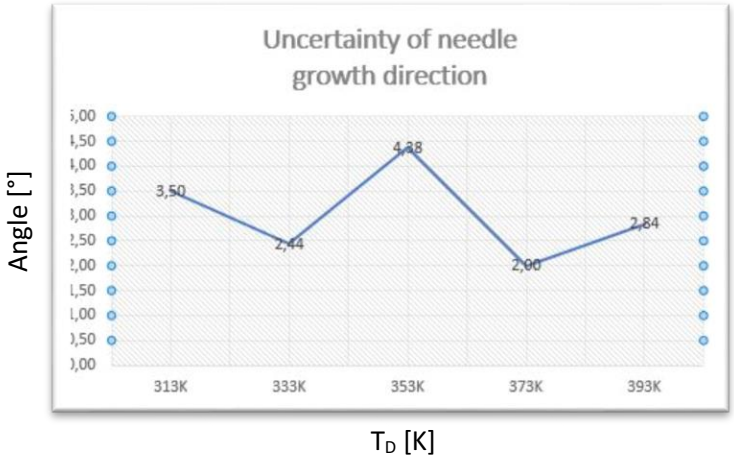

Figure 21: Dependence of angle variations on different T_D.

4.5. Epitaxial relation of DHTA7 and graphene

The Epitaxial relation between DHTA7 and graphene has been obtained by first principle calculations within the framework of the density functional theory (DFT) [47], and analysis of the preferred growth directions obtained from AFM. All of the DFT calculations were carried out by the group of Professor Peter Puschnig (Karl-Franzens-Universität Graz, Austria). All the calculations have been performed using the VASP open-source code. Only single DHTA7 molecules on graphene and two molecules confined in a plane (without substrate) were considered. Periodic boundary conditions and repeated slabs (in z direction, with 1.7 nm of a vacuum layer between the slabs) were used. During the geometry optimization, the DHTA7 molecules and the graphene layer were allowed to fully relax. In order to account for van-der-Waals interactions, the Tkatchenko-Scheffler scheme [45] during the geometry optimization was employed. The results are summarized in Figure 22.

DFT calculations show that the preferred adsorption site is with the long molecular axis (LMA) in the zigzag direction of graphene for single DHTA7 molecule on graphene, see Figure 22 (a). It can also be seen that center of the phenyl rings of DHTA7 are on top of carbon atoms in graphene, so called AB, or Bernal stacking. The nearest high-symmetry adsorption site in a zigzag direction is less favored by about 40 meV, while the nearest high-symmetry adsorption site in an armchair direction is less favored by about 50 meV. These differences between both adsorption sites are expected to be sufficient to keep individual molecules always aligned with their LMA along the zigzag direction of graphene.

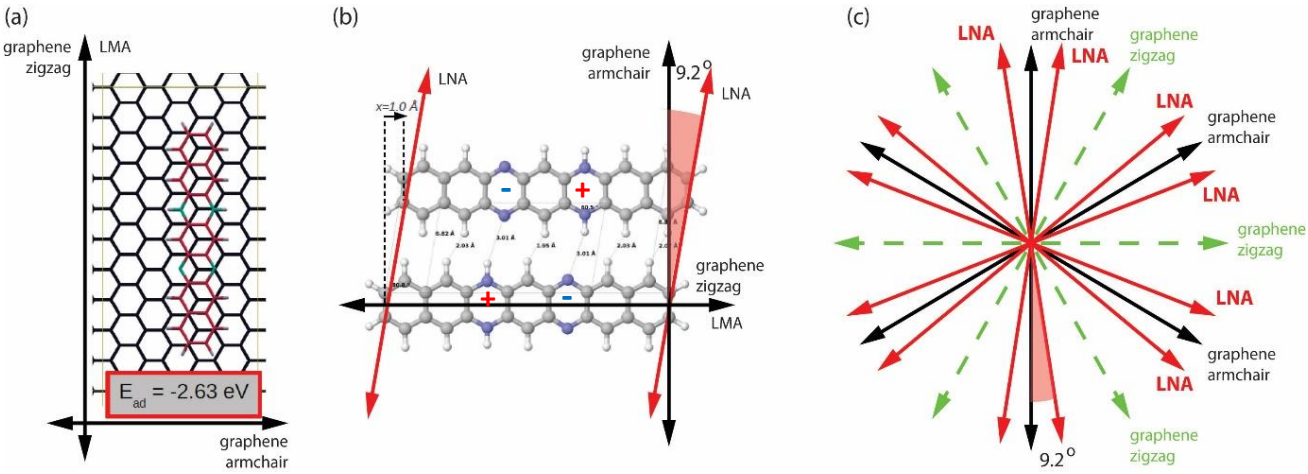

Figure 22: (a) Preferred adsorption site for an individual DHTA7 molecule on graphene. (b) Most stable configuration for two DHTA7 molecules confined in plane. (a) and (b) results from DFT calculations. (c) All possible preferred growth directions of DHTA7 needles on graphene.

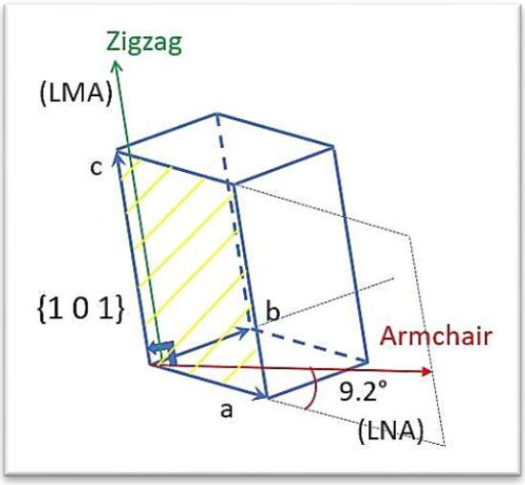

Figure 23: Hypothetical monoclinic unit cell which shows a zigzag direction parallel to the long molecule axis (LMA) while an armchair direction with a tilt of about 9.2° respect to the long needle axis (LNA). Considering the "ac" plane as contact plane between DHTA7 molecules and graphene, which is indicated by planes {1 0 1}.

However, it is not enough to determine the growth directions of the needles with respect to the high symmetry direction of graphene with knowing that LMA is along to the zigzag direction of graphene. When the structures are thicker than one monolayer, the epitaxial relation between the molecules and the substrate could be a compromise between individual adsorption sites (Figure 22 (a)) and the

bulk structure of the molecular crystal. Unfortunately, the bulk structure of the novel molecule DHTA7 is not yet known. It is expected that the molecules form a crystal by π-π stacking, which significantly simplifies the potential candidates for the contact planes of DHTA7 with graphene, since molecules should lay flat on the substrate surface. Figure 22b shows DFT calculations for two DHTA7 molecules fixed in a plane, and their relative position is varied to minimize the total energy of the system. As can be seen from this figure, the molecules do not stack exactly parallel to each other, but are rather shifted. Considering monoclinic cell which is shown in Figure (23), this shift gives a tilt of the "ab" plane with respect to the "bc" plane of 99.2°. Because molecules would lay down on the substrate only if the "ac" plane is the contact plane, this leads to four equivalent contact planes: (1 0 1), (-1 0 1), (1 0 -1) and (-1 0 -1). Next, considering that the long needle axis (LNA) lies in "ab" plane, this possible contact plane family {1 0 1} would also explain the observed splitting of the needle growth directions in the previous chapters. Due to the graphene symmetry, mainly mirror planes and the 3-fold symmetry along armchair directions lead to six preferred growth directions with pairs of directions splitting around three "armchair" directions by about ± 9°. Possible growth directions are shown in Figure 22 (c). Knowing the epitaxial relation between graphene and DHTA7 can be used to determine the type of the edges of graphene flakes, as will be shown in the following paragraph.

4.6 Determining the type of graphene edges

The graphene edge type is important for understanding and controlling the growth of high quality- and large area single crystal graphene using chemical vapor deposition (CVD). For CVD growth of graphene, the armchair edge is a preferred adsorption site for incoming C atoms [48]. Edge termination of grains and nanostructures is very important for their properties [49]. Properties of graphene nanoribbons and nanoflakes can be completely altered by the edge termination. As an example, even slightest edge distortion or termination by any other species than hydrogen can change the bandgap of the nanoribbon more than 1 eV [50]. Further, if the edges of a nanoribbon are perfect there will be significant difference of the properties depending on the edge type, and unique spin states and semi-metallic behavior are appearing in zigzag terminated graphene nanoribbons, which do not exist in armchair ribbons of same width [51].

Figure 24 represents the orientations of DHTA7 needles grown on a few-layer graphene flakes at T_D of 333K. Hypothesis is that sharp edges of the flake of which directions are separated by an integer multiple of 30°, are either armchair or zigzag. From the needle growth directions, it is possible to determine the crystallographic orientation of the supporting graphene flake, as is indicated in Figure 24 (a) by the solid red and green lines (armchair and zigzag) which are parallel to the flake edges.

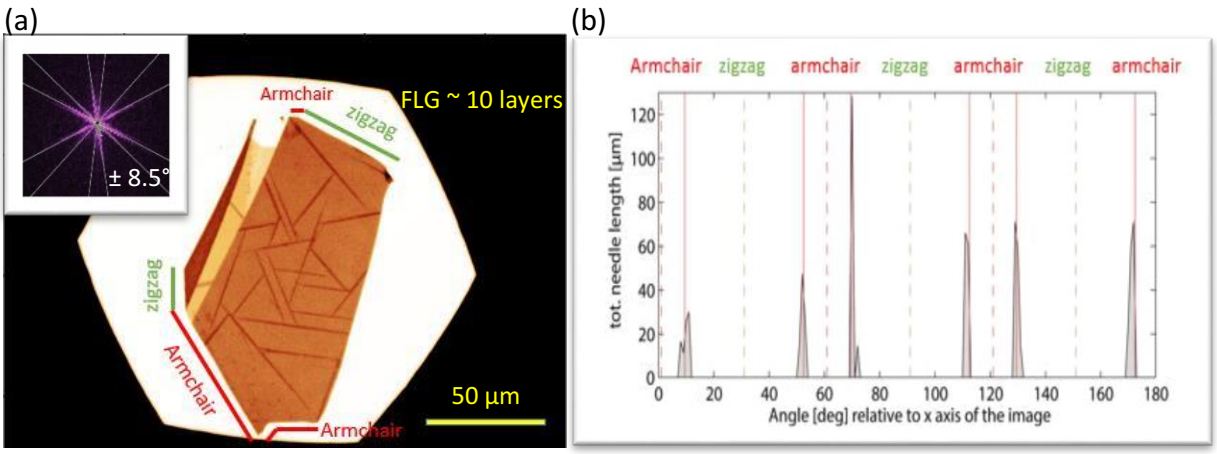

Figure 24 (a): Optical microscopy images at 500x magnification of bulk FLG graphene flakes with DHTA7 needles (T_D = 333K). Insert in (a): Corresponding 2D FFT image with an angle between each two solid lines of about 17°. (b): Histogram of angular distribution corresponding to (a) with ±1° accuracy. Dashed red and green lines in (b) indicate armchair and zigzag directions of the graphene flake respectively. Solid red lines represent ± 8.5° splitting from armchair directions of graphene flakes.

4.7 Influence of graphene thickness on the growth morphologies

For rod-like molecules grown on graphene, the effects of a water layer induced dipole field on the growth of organic semiconductors has been investigated earlier and are presented in figure 25. It can be noticed that a trapped water layer significantly affects the growth of rod-like molecules on graphene. Morphology changes from upright standing islands, when a water layer is present, to flat-lying needles when this layer is suppressed [52]. Figure 25 (a) also illustrates an opposite tendency of DHTA7 needle growth for an increase of supporting flake thickness. This is attributed to the changes in surface energy of graphene with additional layers.

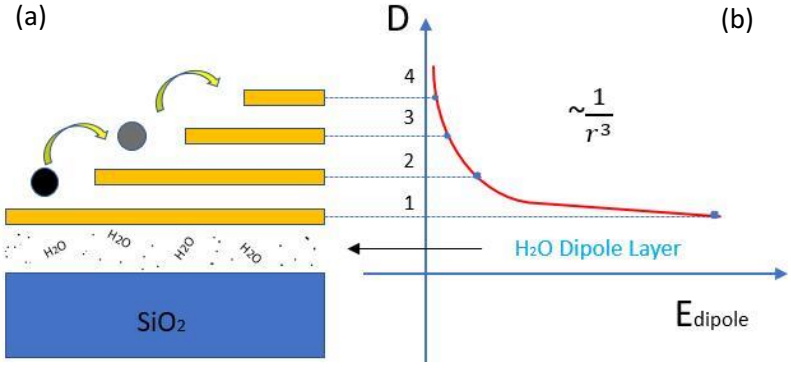

Figure 25: (a) Schematic of the interface between graphene and SiO_2. (b) Illustrative plot of the variation in surface potential E (screening of the interfacial dipole field with graphene layers), versus graphene thickness D, if considering independent dipoles where the decay of the field is $\sim\frac{1}{r3}$.

As can be seen from Figure 26 (a), for the distribution of needle-like structures on top of different graphene layers, there is almost no existence of needles on the surface of SLG (monolayer). The needles seem “to avoid” nucleating and growing on both SLG areas. Moreover, a different situation can be noticed in Figure 26 (b) where needles did nucleate on top of SLG. A possible explanation for the difference observed in 26 (a) and (b) is the fact that the molecules will nucleate on SLG only if they have no other option (no nearby multi-layer structures), as in the case of only SLG flakes. In the case presented in Figure 26, both flakes were on the same Si/SiO_2 substrate, which should give very comparable parameters for both flakes, since both flakes were made in the same exfoliation process, and the molecules were grown under the same conditions. Also, it can be observed that the molecules on SLG form shorter and more disordered needles compared to the BLG and TLG case.

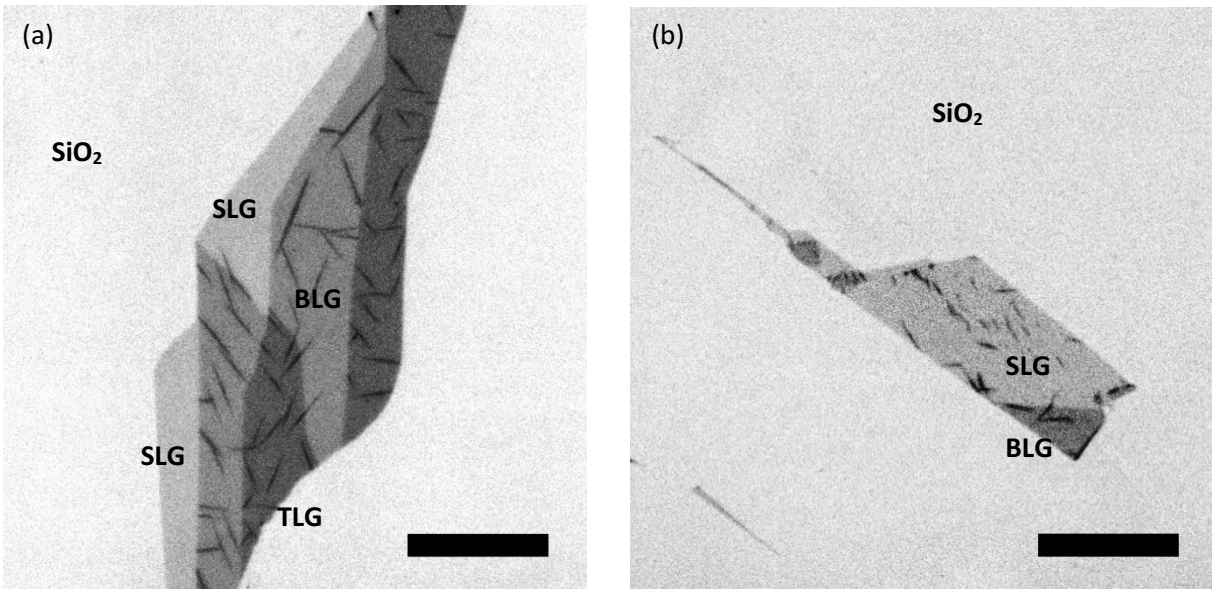

Figure 26: Optical microscopy images at 1000x magnification of graphene flakes with DHTA7 needles at a deposition temperature of 333K. Lateral scales bar: 15 µm. (a) Flake consisting of single-layer graphene (SLG), bi-layer (BLG) and tri-layer (TLG) with distinct areas. (b) Flake with almost only SLG.

4.8 Influence of graphene surface contaminations on the DHTA7 morphologies

Graphite is usually considered as an inert surface, since its vdW nature has no dangling bond that would act as anchoring sites for chemisorption of the surface contaminates. However, in ambient conditions graphite still accumulates physiosorbed species on the surface, especially hydrocarbon based compounds. Usually a clean surface of layered materials is obtained by a cleavage procedure using adhering scotch tape to the top surface and removing the top layers from the bulk crystal, thus

leaving a fresh surface behind that had not previously been exposed to the air or any other contaminates of the exfoliation process (e.g. glue within the tape or liquids used within micromechanical exfoliation process). While this method is used to obtain "clean" 2D materials, organic contaminants can adsorb on the surface if the process is not carried out in vacuum despite the inert nature of the materials [53]. For this reason, to minimize the contaminations due to air exposure, a second exfoliation step has been performed in high vacuum. Thus, the molecules are grown without breaking the vacuum environment. An example is shown in Figure 27 (a), where area "A" indicates a first exfoliated surface (in air, and with exfoliation contaminants) and "B" a second

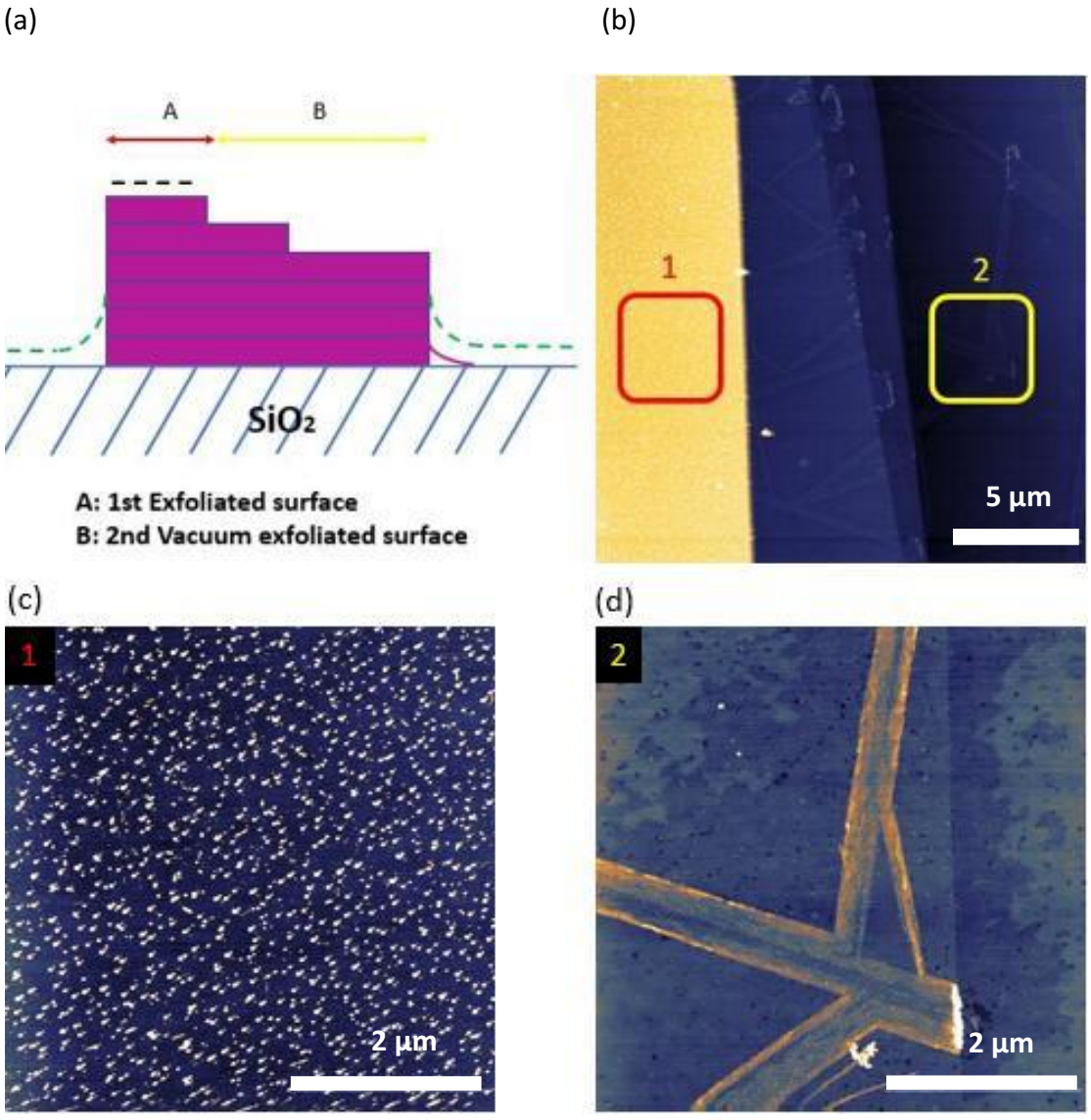

Figure 27: (a) Schematic of a graphite flake on top of SiO_2 with two parts of surfaces "A and B" after different exfoliation methods. (b), (c), (d) 20 x 20 μm^2 AFM image of DHTA7 morphology on graphite corresponding to figure (a). 5 x 5 μm^2 AFM images which correspond to the two small areas "1 and 2" in Figure (b). Z scales: 40 nm (b), 5 nm (c), and (d).

vacuum exfoliated surface as well. The contaminants on the surface “A” of graphite after first exfoliation is indicated by the black dashed line in (a). As a contrast, “B” is the surface prepared in high-vacuum by an additional exfoliation step and thus has a minimal surface contamination as possible in this case. After the deposition of molecules on it, the DHTA7 morphologies were investigated using AFM. An overview AFM topography image of the graphite sample, which contains both the first exfoliation (left) and second-vacuum exfoliation (right) surfaces is shown in figure 27(b). Red and blue squares in figure 27(b) correspond to enlarged areas (show in figure 27(c,d)) of the contaminated (“A”) and clean (“B”) surfaces, respectively. On the surface “B”, well ordered needle-like structures of DHTA7 are found. On the other hand, the morphology on the surface “A” is strikingly different with very short and tall needle-like structures, not large enough to resolve any preferred growth directions. This is shown in figure 27(c,d), where “zoom-in” AFM topography images of these two areas are presented. The magnification of surface morphology corresponding to “area 1” is revealed in figure 27(c). Here, most likely surface contaminations induce the nucleation and many small 3D structures are grown. An ordered needle-like structure of DHTA7 was found on the clean surface of graphite, which is clearly seen in figure 27(d). Since these two different structures of DHTA7 were found on the same flake, influences like different growth conditions can be neglected. The only difference that remains is that the surface on which the well-ordered structures were found was prepared in high-vacuum and not exposed to air. As such, second surface should be very clean with negligible amounts of adsorbates prior to the growth of the molecules.

This example demonstrates the necessity to know - and control – the cleanliness of the substrate surface prior to the growth since surface contaminations can severely alter the morphology of the grown crystallites, especially in the case of polar molecules as DHTA7 on vdW materials.

5. Conclusions

In summary, the growth of the novel, polar molecule dihydrotetraazaheptacene (DHTA7) on graphene and graphite has been analyzed. The chosen molecular species are dipolar and form hydrogen bridges, which both contribute to a high stability of the crystallites in ambient conditions. This is in contrast to heptacene – and even pentacene – which are not stable under ambient conditions. Micromechanical exfoliations have been used to prepare high-quality atomic layer graphene on SiO_2/Si wafers, which both serve as substrates for the growth of the molecules. Deposition of DHTA7 molecules was achieved through the hot wall epitaxy technology. To examine the growth behavior of DHTA7 supported by graphene and graphite, atomic force microscopy in tapping mode as well as optical microscopy have been employed. The analysis of topography data was realized by software Gwyddion.

From the observed needle like morphologies it was derived that DHTA7 molecules are adsorbed in a flat-lying configuration on graphene and graphite, in contrast to an up-right standing configuration (as island-like crystallites) on SiO_2. The dependence of the DHTA7 crystallites' morphology on the deposition temperature has been analyzed in the thesis within a range for T_D between 313 K and 393 K. With proper growth parameters, needles can grow unperturbed across entire flakes, yielding high geometrical aspect ratios of these self-assembled crystallites. Films grown at 333 K exhibit needles over 20 µm in length with aspect ratios: length/width > 1000, and length/height >100000. In addition, needles found on graphene and graphite have clearly preferred growth directions. This self-organization is governed by the molecule-substrate interaction, and the directions are determined by epitaxial relation between them. Using additional information – as preferential adsorption sites obtained by first-principle calculations – it was possible even to reconstruct the crystallographic orientation of the underlying substrate. The 3-fold symmetry along armchair directions leads to six preferred growth directions of needles, with pairs of directions split around three "armchair" directions by about ± 9°, and each pair separated by 60°.

Finally, the influence of the graphene thickness on the growth morphologies was also demonstrated. Single-layer graphene was found not to be preferred for the growth of DHTA7 needles on top of it. This is most likely due to the interface dipoles induced by a trapped water layer at graphene/SiO_2 interface. The needles seem to avoid nucleating and growing on single-layers if possible and do nucleate on these flakes only if there are no nearby multi-layer graphene structures on to which the molecules could diffuse.

The novel findings presented in this thesis are important to understand the growth behavior of dipolar rod-like organic semiconductors on van der Waals materials. The findings could lead to further optimization of these interfaces and to future application of them in the fields of flexible electronics, in particular for flexible lighting, flexible solar cells, and flexible screens.

Knowing how molecules grow on a desired substrate is a basis for further research and understanding of their interface, which will help target appropriate potential applications. In this particular case of an interface between DHTA7 and graphene, understanding the growth behavior will allow future studies that can investigate the band alignment and the charge transfer at this interface, enabling efficient charge injection through the interface. Furthermore, self-assembled needles of DHTA7 on graphene have very large aspect ratios, and gaining external control over their preferred growth directions could lead to advance bottom-up fabrication techniques. As an idea, since the molecules are dipolar, it is reasonable to assume that externally applied electric fields could guide the growth of the needles.

Acknowledgements

I would like to express my thanks of gratitude to:

Ao.Univ.-Prof. Dipl.-Phys. Dr.rer.nat. Christian Teichert, my advisor, for his instructive advice and great suggestion on my thesis, for giving me the golden opportunity to do this wonderful research, for his kind and excellent supervision, for extending my outlook of material science study.

Dr. Dipl.inz.elektr. Aleksandar Matković, my co-advisor, for the irreplaceable help with my thesis, for teaching me about the cognition and operation of AFM and other equipment, preparing the graphene samples and growing the DHTA7 molecules, for his useful suggestion on the figures, kind and patient support and careful correction of this thesis.

Prof. Olivier Siri, and Dr. Zhongrui Chen, CINAM-CNRS, Aix - Marseille – University for providing the novel, dipolar molecule DHTA7.

Prof. Dr. Peter Puschnig, Karl – Franzens – University Graz for DFT calculations of DHTA7.

The Austrian Science Fund (FWF) for financial support through a joint French-Austrian project ANR-FWF, project number: I1788-N20.

Heide Kirchberger and Tomas Jud for administrative support.

Dipl.-Ing. Dr.techn. Markus Kratzer, Dipl.-Ing. Caterina Czibula, Dr.mont. Christian Ganser, Dipl.-Ing. Jakob A. Genser, Aydan Cicek and Kevin Gradwohl for their selfless help and the nice working atmosphere.

All of my family, especially my wife and my parents for their loving considerations and great confidence in me all through these years.

My friends and colleagues

List of acronyms

2D	two-dimensional
AFM	atomic force microscopy
DFT	density functional theory
DHTA7	dihydrotetraazaheptacene
DHTAP	dihydrotetraazapentacene
FET	field-effect transistor
FFT	Fast Fourier Transform
FWHM	full width at half maximum
HWE	Hot Wall Epitaxy
LMA	long molecule axis
LNA	long needle axis
OFET	organic field-effect transistor
OLED	organic light emitting diode
OSC	organic semiconductor
T_D	deposition temperature
vdW	van der Waals

References

[1] Novoselov K. S., Geim A. K., Morozov S. V., Jiang D., Zhang Y., Dubonos S. V., Grigorieva I. V., and Firsov A. A., Electric field effect in atomically thin carbon films, *Science* **306** (2004) 666-669.

[2] Geim A. K., Grigorieva I. V., Van der Waals heterostructures, *Nature* **499** (2013) 419-425.

[3] Ferrari A. C, et.al., Science and technology roadmap for graphene, related two-dimensional crystals, and hybrid systems, *Nanoscale* **7** (2015) 4598-4810.

[4] Bullis K., Mass production of plastic solar cells, *MIT Technology Review*, (2008), Retrieved from: http://www. technologyreview. com/energy/21574/page1.

[5] Ruiz R., Papadimitratos A., Mayer A. C., and Malliaras G. G., Thickness Dependence of Mobility in Pentacene Thin-Film Transistors, *Advanced Materials* **17** (2005) 1795-1798.

[6] Mühlenen A., Castellani M., Schaer M., and Zuppiroli L., Controlling charge-transfer at the gate interface of organic field-effect transistors*, Physica Status Solidi* **245** (2008) 1170-1174.

[7] Image taken from: https://www.azonano.com/article.aspx?ArticleID=4454.

[8] Balandin A. A., Thermal properties of graphene and nanostructured carbon materials, *Nature Materials* **10** (2011) 569-581.

[9] Nair R. R., Blake P., Grigorenko A. N., Novoselov K. S., Booth T. J., Stauber T., Peres N. M. R., and Geim A. K., Fine structure constant defines visual transparency of graphene, *Science* **320** (2008) 1308-1308.

[10] http://www.telegraph.co.uk/travel/news/graphene-is-the-future-of-aircraft-technology/

[11] Sun S., Gao L., and Liu Y., Enhanced dye-sensitized solar cell using graphene-TiO_2 photoanode prepared by heterogeneous coagulation, *Applied Physics Letters* **96** (2010) 083113.

[12] Koma A., Van der Waals epitaxy for highly lattice-mismatched systems, *Journal of Crystal Growth* **201** (1999) 236-241.

[13] Di C., Wei D., Yu G., Liu Y., Guo Y., and Zhu D., Patterned Graphene as Source/Drain Electrodes for Bottom-Contact Organic Field-Effect Transistors, *Advanced Materials* **20** (2008) 3289.

[14] Pang S., Tsao H. N., Feng X., and Müllen K., Patterned graphene electrodes from solution-processed graphite oxide films for organic field-effect transistors, *Advanced Materials* **21** (2009) 3488.

[15] Lee W. H., Park J., Sim S. H., Lim S., Kim K. S., Hong B. H., and Cho K., Surface-directed molecular assembly of pentacene on monolayer graphene for high-performance organic transistors, *Journal of the American Chemical Society* **133** (2011) 4447.

[16] Lee C. H., et. al., Epitaxial Growth of Molecular Crystals on van der Waals Substrates for High-Performance Organic Electronics, *Advanced Materials* **26** (2014) 2812-2817.

[17] Kuruvila A., Kidambi R. P., Kling J., Wagner J. B., Robertson J., Hofmann S., and Meyer J., Organic light emitting diodes with environmentally and thermally stable doped graphene electrodes, *Journal of Materials Chemistry C* **2** (2014) 6940.

[18] Meyer J., Kidambi P. R., Bayer B. C., Weijtens C., Kuhn A., Centeno A., Pesquera A., Zurutuza A., Robertson J., and Hofmann S., Metal oxide induced charge transfer doping and band alignment of graphene electrodes for efficient organic light emitting diodes, *Scientific Reports* **4** (2014) 5380.

[19] Sanders S., Vilatela A. C., Kidambi P.R., and Meyer J., Engineering high charge transfer n-doping of graphene electrodes and its application to organic electronics, *Nanoscale* **7** (2015) 13135.

[20] Kidambi P. R., Weijtens C., Robertson J., Hofmann S., and Meyer J., Multifunctional oxides for integrated manufacturing of efficient graphene electrodes for organic electronics, *Applied Physics Letters* **106** (2015) 20.

[21] Han K. S., Kalode P. Y., Lee Y. K., Kim H., Lee L., and Sung M. M., A non-destructive n-doping method for graphene with precise control of electronic properties via atomic layer deposition, *Nanoscale* **8** (2016) 5000.

[22] Liu X., Luo X., Nan H., Guo H., Wang P., Zhang L., Zhou M., Yang Z., Shi Y., Hu W., Ni Z., Qiu T., Yu Z., Xu J., and Wang X., Epitaxial Ultrathin Organic Crystals on Graphene for High-Efficiency Phototransistors, *Advanced Materials* **28** (2016) 5200-5205.

[23] Lelaidier T., Leoni T., Arumugam P., Ranguis A., Becker C., and Siri O., Highly Ordered Molecular Films on Au (111): The N-Heteroacene Approach, *Langmuir* **30** (2014) 5700-5704.

[24] Di C., Li J., Yu G., Xiao Y., Guo Y., Liu Y., Qian X. and Zhu D., Trifluoromethyltriphenodioxazine: air-stable and high-performance n-type semiconductor, *Organic Letters* **10** (2008) 3025-3028.

[25] Maliakal A., Raghavachari K., Katz H., Chandross E., and Siegrist T., Photochemical stability of pentacene and a substituted pentacene in solution and in thin films, *Chemistry of Materials* **16** (2004) 4980-4986.

[26] Bunz H. F., Engelhart J. U., Lindner B. D., and Schaffroth M., Large N-Heteroacenes: New Tricks for Very Old Dogs, *Angewandte Chemie International Edition* **52** (2013) 3810-3821.

[27] Tang Q., Liu J., Chan H. S., Miao Q., Benzenoid and Quinonoid Nitrogen-Containing Heteropentacenes, *Chemistry-A European Journal* **15** (2009) 3965-3969.

[28] M Y., et al., From zero to two dimensions: supramolecular nanostructures formed from perylene-3, 4, 9, 10-tetracarboxylic diimide (PTCDI) and Ni on the Au (111) surface through the interplay between hydrogen-bonding and electrostatic metal-organic interactions, *Nano Research* **5** (2012) 903-916.

[29] Krane N., Preparation of graphene, Selected Topics in Physics: *Physics of Nanoscale Carbon – Freie Universität Berlin, Germany*, (2011). Retrieved from: http://www.physik.fu-berlin.de/

[30] Casiraghi C., Hartschuh A., Lidorikis E., Qian H., Harutyunyan H., Gokus T., Novoselov K. S., and Ferrari A. C., Rayleigh imaging of graphene and graphene layers. *Nano letters* **7** (2007) 2711-2717.

[31] Scheme of exfoliation, courtesy of A. Matković.

[32] Sadeghi M., Sitter H., and Gruber H., Epitaxial growth of thin GaAs layers by hot-wall epitaxy on transparent substrates, *Journal of Crystal Growth* **70** (1984) 103-107.

[33] Frey H., Hartmut H. R., *Handbook of thin film technology*, Ed. Khan. H. R., Springer-Verlag Berlin Heidelberg, (2015).

[34] Lopez-Otero A., Hot wall epitaxy, *Thin solid Films* **49** (1978) 3-57.

[35] Blake P., Hill E. W., Castro A. H., Novoselov K. S., Jiang D., Yang R., Booth T. J., and Geim A. K., Making graphene visible, *Applied Physics Letters* **91** (2007) 063124.

[36] Ferrari A. C., Meyer J. C., Scardaci V., Casiraghi C., Lazzeri M., Mauri F., Piscanec S., Jiang D., Novoselov K. S., Roth S., and Geim A. K., Raman spectrum of graphene and graphene layers, *Physical Review Letters* **97** (2006) 187401.

[37] Novoselov K. S., and Geim A. K., The rise of graphene, *Nature Material* **6** (2007), 183.

[38] https://www.microscopyu.com/techniques/phase-contrast/specimen-contrast-in-optical-microscopy

[39] Meyer E., Hug H. J., and Bennewitz R., *Scanning probe microscopy: the lab on a tip*, Springer-Verlag Berlin Heidelberg New York, (2004).

[40] https://en.wikipedia.org/wiki/Atomic-force_microscopy

[41] Eaton P., and West P., *Atomic force microscopy*, Oxford University Press Inc., New York, (2010).

[42] Zhong Q., Inniss D., Kjoller K., and Elings V.B., Fractured polymer/silica fiber surface studied by tapping mode atomic force microscopy, *Surface Science* **290** (1993) L688-L692.

[43] Nečas D., and Klapetek P., Gwyddion: an open-source software for SPM data analysis*, Open Physics* **10** (2012) 181-188.

[44] Hlawacek G., Puschnig P., Frank P., Winkler A., Ambrosch C., and Teichert C., Characterization of step-edge barriers in organic thin-film growth, *Science* **321** (2008) 108-111.

[45] Matković A., Genser J., Lüftner D., Kratzer M., Gajić R., Puschnig P., and Teichert C., Epitaxy of highly ordered organic semiconductor crystallite networks supported by hexagonal boron nitride, *Scientific Reports* **6** (2016) 38519.

[46] Kratzer M., and Teichert C., Thin film growth of aromatic rod-like molecules on graphene, *Nanotechnology* **27** (2016) 292001.

[47] Kohn W., Nobel Lecture: Electronic structure of matter—wave functions and density functionals, *Reviews of Modern Physics* **71** (1999) 1253.

[48] Luo Z., Kim S., Kawamoto N., Rappe A. M., and Johnson A. T., Growth mechanism of hexagonal-shape graphene flakes with zigzag edges, *ACS Nano* **5** (2011) 9154-9160.

[49] Jia X., Hofmann M., Meunier V., Sumpter B.G., and Dresselhaus M.S., Controlled formation of sharp zigzag and armchair edges in graphitic nanoribbons, *Science* **323** (2009) 1701-1705.

[50] Evaldsson M., Zozoulenko I. V., Xu H., and Heinzel T., Edge-disorder-induced Anderson localization and conduction gap in graphene nanoribbons, *Physical Review B* **78** (2008) 161407.

[51] Son Y. W., Cohen M. L., and Louie S. G., Half metallic graphene nanoribbons, *Nature* **444** (2006) 347–349.

[52] Chhikara M., Pavlica E., Matković A., Beltaos A., Gajić R., and Bratina G., Pentacene on graphene: Differences between single layer and bilayer, *Carbon* **69** (2014) 162-168.

[53] *2D Materials for Nanoelectronics*, Ed.-s Houssa M., Dimoulas A., and Molle A., Series in Materials Science and Engineering, CRC Press, Taylor & Francis Goup, Boca Raton London New York, (2016).